Synthesis of adenine dinucleosides SAM analogs as specific inhibitors of SARS-CoV nsp14 RNA cap guanine-N7-methyltransferase

Rostom Ahmed-Belkacem, Priscila Sutto-Ortiz, Mathis Guiraud, Bruno Canard, Jean-Jacques Vasseur, Etienne Decroly, Françoise Debart

Since January 2020 Elsevier has created a COVID-19 resource centre with free information in English and Mandarin on the novel coronavirus COVID-19. The COVID-19 resource centre is hosted on Elsevier Connect, the company's public news and information website.

European Journal of Medicinal Chemistry 201 (2020) 112557

Contents lists available at ScienceDirect

European Journal of Medicinal Chemistry

journal homepage: http://www.elsevier.com/locate/ejmech

Research paper

Synthesis of adenine dinucleosides SAM analogs as specific inhibitors of SARS-CoV nsp14 RNA cap guanine-N7-methyltransferase

Rostom Ahmed-Belkacem [a], Priscila Sutto-Ortiz [b], Mathis Guiraud [a], Bruno Canard [b], Jean-Jacques Vasseur [a], Etienne Decroly [b, **], Françoise Debart [a, *]

[a] IBMM, CNRS, University of Montpellier, ENSCM, Montpellier, France
[b] AFMB, CNRS, Aix-Marseille University, UMR 7257, 163 Avenue de Luminy, Marseille, France

ARTICLE INFO

Article history:
Received 7 May 2020
Received in revised form
26 May 2020
Accepted 8 June 2020
Available online 12 June 2020

Keywords:
Nucleoside
Bisubstrate
SAM analogs
Coronavirus
RNA methyltransferase
Inhibitor

ABSTRACT

The spreading of new viruses is known to provoke global human health threat. The current COVID-19 pandemic caused by the recently emerged coronavirus SARS-CoV-2 is one significant and unfortunate example of what the world will have to face in the future with emerging viruses in absence of appropriate treatment. The discovery of potent and specific antiviral inhibitors and/or vaccines to fight these massive outbreaks is an urgent research priority. Enzymes involved in the capping pathway of viruses and more specifically RNA N7- or 2′*O*-methyltransferases (MTases) are now admitted as potential targets for antiviral chemotherapy. We designed bisubstrate inhibitors by mimicking the transition state of the 2′-*O*-methylation of the cap RNA in order to block viral 2′-*O* MTases. This work resulted in the synthesis of 16 adenine dinucleosides with both adenosines connected by various nitrogen-containing linkers. Unexpectedly, all the bisubstrate compounds were barely active against 2′-*O* MTases of several flaviviruses or SARS-CoV but surprisingly, seven of them showed efficient and specific inhibition against SARS-CoV N7-MTase (nsp14) in the micromolar to submicromolar range. The most active nsp14 inhibitor identified is as potent as but particularly more specific than the broad-spectrum MTase inhibitor, sinefungin. Molecular docking suggests that the inhibitor binds to a pocket formed by the S-adenosyl methionine (SAM) and cap RNA binding sites, conserved among SARS-CoV nsp14. These dinucleoside SAM analogs will serve as starting points for the development of next inhibitors for SARS-CoV-2 nsp14 N7-MTase.

1. Introduction

Emerging RNA viruses are serious threats to public health and have become a worldwide concern. The violent Ebola virus crisis in 2014 [1] (case fatality rate ≈ 50%) and the recurrent outbreaks of Coronaviruses in 2003 (SARS-CoV, case fatality rate ≈ 10% [2]), in 2012 (MERS-CoV, case fatality rate ≈ 36% [3]) and in late december 2019 (SARS-CoV-2) [4] illustrate the critical impact of such viruses. The ongoing COVID-19 pandemic caused by the recently emerged new coronavirus, SARS-CoV-2 [4], is a global health crisis touching every continent (187 countries) with severe economic impact. Most infected people display mild to moderate respiratory illness however patients having co-morbidity factors develop serious illness and pneumonia causing significant mortality [5,6]. This disease endangers 7.7 billion people worldwide with in may 2020 more than 5.3 millions of confirmed cases of infected people and more than 350,000 confirmed deaths, and the number of COVID-19 cases will certainly progress in the next months with a possible rebond of the epidemic [7]. Despite this important public health threat, there are no yet approved chemotherapeutic agents or vaccines that can prevent or cure infections. Therefore, the urgent need of antivirals limiting the coronavirus propagation merits intensive efforts.

Most of single positive strand RNA viruses have evolved strategies in order to decorate the 5′ end of their own genome by a cap

Abbreviations: SARS, severe acute respiratory syndrome coronavirus; MERS, Middle East respiratory syndrome; CoV, coronavirus; COVID19, coronavirus disease 2019; MTase, methyltransferase; nsp14, non-structural protein 14; SAM, *S*-adenosyl methionine; hRNMT, human RNA methyltransferase; Ns-amide, nitrobenzenesulfonamide; DSF, diffraction scanning fluorimetry; FBA, filter binding assay.

* Corresponding author.
** Corresponding author.
E-mail addresses: etienne.decroly@afmb.univ-mrs.fr (E. Decroly), francoise.debart@umontpellier.fr (F. Debart).

https://doi.org/10.1016/j.ejmech.2020.112557
0223-5234/

structure mimicking the eukaryotic messenger RNA. This structure plays several key biological functions such as protection of RNA from 5′-exoribonucleoases and initiation of the RNA translation into proteins. Moreover the cap is a marker of 'self' preventing detection by the cellular innate immunity mechanism. Thus viruses such as flaviviruses and coronaviruses code for RNA capping pathway mimicking that of eukaryotic cells. These viruses produce a subset of enzymatic activities including a RNA 5′-triphosphatase, a guanilyltransferase (GTase) and two RNA cap methyltransferases (MTases) [8]. After the cap (GpppN) is set by the GTase, a first methylation occurs at N7 position of the guanine by a N7-MTase in the presence of methyl donor S-adenosyl methionine (SAM) yielding to a cap-0 (^{7m}GpppN) followed by a further methylation that is achieved by a 2′-*O*-MTase at 2′- position of the ribose of the first transcribed nucleotide in RNA yielding cap-1 (^{7m}GpppN$_m$) (Scheme 1). The N7- and 2′-*O*-methylation of the viral RNA cap are key events for the viral infection as their inhibition might limit the synthesis of viral proteins and support virus elimination by stimulation of the immune response [9]. Therefore it is now admitted that the viral MTases are considered as attractive targets for the development of antiviral therapy [10,11]. Few viral MTase inhibitors have been developed so far, however SAM-mimetics acting as competitors against the MTase co-substrate merit attention. Indeed SAM analogs such as sinefungin, 5′-methylthioadenosine (MTA) or S-adenosyl homocysteine (SAH) inhibit most of viral MTases with a potent efficiency but with a total lack of specificity [12]. This is certainly due to the high conservation of the shape and location of the SAM binding pocket in the human or different viral RNA MTases which share a common Rossman fold organization [13]. The rarity of specific inhibitors for viral MTases constitutes a stimulating challenge for new antiviral therapy but also for functional studies of these fascinating enzymes.

With the aim of enhancing specificity of MTase inhibitors, we developed an approach of bisubstrate inhibitors that display a suitable linker between two adenosines that mimic the transition state of the methyl transfer reaction at 2′-*O* position of the RNA cap structure [12]. One adenosine is supposed to target the SAM binding site and another adenosine would target the RNA binding site (Fig. 1). Recently, we described the synthesis of a first series of bisubstrate adenine dinucleosides with various sulfur-containing linkers [14]. Unexpectedly, such compounds tested at 50 μM or 200 μM concentration failed to inhibit several RNA 2′*O*-MTases of SARS-CoV, Zika, West Nile, Dengue and Pox viruses such as vaccinia virus. Their potential of inhibition toward N7-MTases of SARS-CoV and vaccinia virus was also explored and none of the *S*-linked dinucleosides was active against these N7-MTases. From these data, in the present work we replaced the sulfur atom (*S*) by a nitrogen

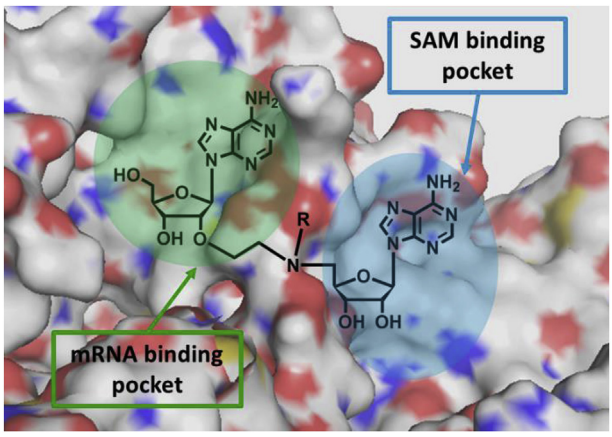

Fig. 1. Rationale for designing a library of bisubstrate compounds for targeting RNA 2′-*O*-methyltransferases.

atom (*N*) in the linker between both adenosines. This modification presents the advantage of increasing the chemical stability of the linker and offers a possible variability of compounds due to the *N*-substitution by any chain susceptible to interact with additional protein residues (Scheme 1). It is noteworthy that bisubstrate dinucleosides with *N*-containing linkers have already been reported in transition state analogs of DNA methylation [15] and of RNA methylation at *N*6 position of adenosine [16,17]. However, till our work, none viral 2′*O*-MTase or N7-MTase have been targeted by bisubstrate adenine dinucleosides. This observation led us to explore the impact of *N*-linkers on the antiviral activity of bisubstrate SAM analogs.

We thus synthesized a new series of transition state analogs of the RNA 2′-*O*-methylation reaction based on the coupling of a 2′-*O*-ethyl adenosine to a 5′-amino adenosine. We explored a variety of *N*-substituted linkers in adenine dinucleosides and their inhibition activity was evaluated against several viral RNA 2′*O*-MTases as well N7-MTases for specificity purpose. Unexpectedly, none of the *N*-linked dinucleosides inhibited any 2′*O*-MTases of flaviviruses or SARS-CoV. However, interestingly some *N*-nitrobenzenesulfonamide-containing dinucleosides were found to specifically inhibit SARS-CoV N7-MTase nsp14 without inhibiting the cognate human N7-MTase or vaccinia N7-MTase. Such specific inhibition results from a high binding affinity of the most potent inhibitors to N7-MTase nsp14. In addition, computational docking analysis identified some residues of the binding site for the best inhibitor targeting nsp14. As SAM and RNA binding sites of N7-

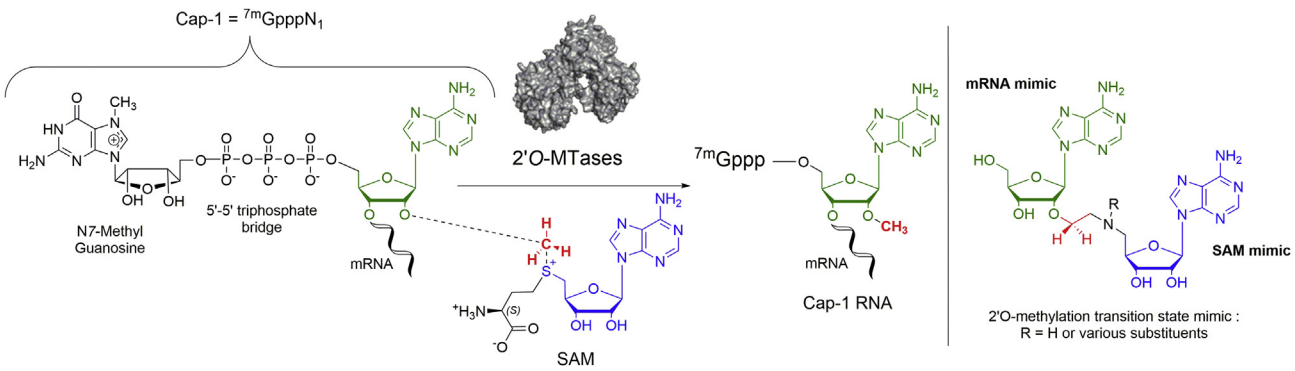

Scheme 1. Schematic representation of the 2′-*O*-methylation of the cap structure at nucleoside N1 at 5′-end of mRNA to form Cap-1 RNA. General structure of compounds mimicking the 2′-*O*-methylation transition state between N1 of mRNA (adenosine in green) and SAM (adenosine in blue).

MTase nsp14 are almost completely conserved between SARS-CoV and SARS-CoV-2 (95% sequence homology, Supporting Info Fig. S1) [18], we can forecast that the candidate ligands that are efficient in inhibiting the SARS-CoV functions will be efficient in doing the same for SARS-CoV-2, this emphasizes the interest of the present work.

2. Results and discussion

2.1. Rational design of bisubstrate compounds

In order to mimic the transition state of the cap RNA 2′-*O*-methylation, the design of the SAM mimetics relies on the coupling of the adenosine moiety of the SAM cofactor to another adenosine modified at 2′-*O*-position with an ethyl group to form the link. Thus, we first synthesized the dinucleoside **1** with a 2′-*O*-ethyl amino link between both adenosines (Scheme 2). The major advantage of this *N*-containing linker is the possibility to functionalize the secondary amine with a large variety of groups which may lead to additional binding with specific sites of RNA 2′-*O*-MTases. According to the schematic representation of the transition state of the 2′-*O*-methylation (Scheme 1), an accurate mimic was represented by compound **2** with the α-amino acid chain of the SAM branched to the nitrogen atom [16]. We further modified this side chain under α-amino-ester form or α-amino-amide form to result in compounds **3** and **4**, respectively. Then instead of polar modifications, we introduced hydrophobic substituents on the secondary amine in dinucleosides **5**, **6** and **7**. Finally we chose to obtain compound **9** with a nitrobenzenesulfonamide moiety as a structural particular element of the dinucleoside. Indeed, as a global observation in medicinal chemistry the *N*-arylsulfonamide motif is regularly found in antitumor agents as in some antiviral inhibitors [19,20]. Further, we explored the combination of the nitro group with another substituent (MeO, CF_3, Cl) at diverse positions in the phenyl ring resulting in the compounds **10**–**13** and we also removed the nitro group in **14** (Scheme 3). In addition, we chose to replace the sulfone by a methylene group in **15**–**16** (Scheme 4) to assess the sulfone contribution to the inhibitory activity obtained with dinucleosides containing the *N*-arylsulfonamide motif.

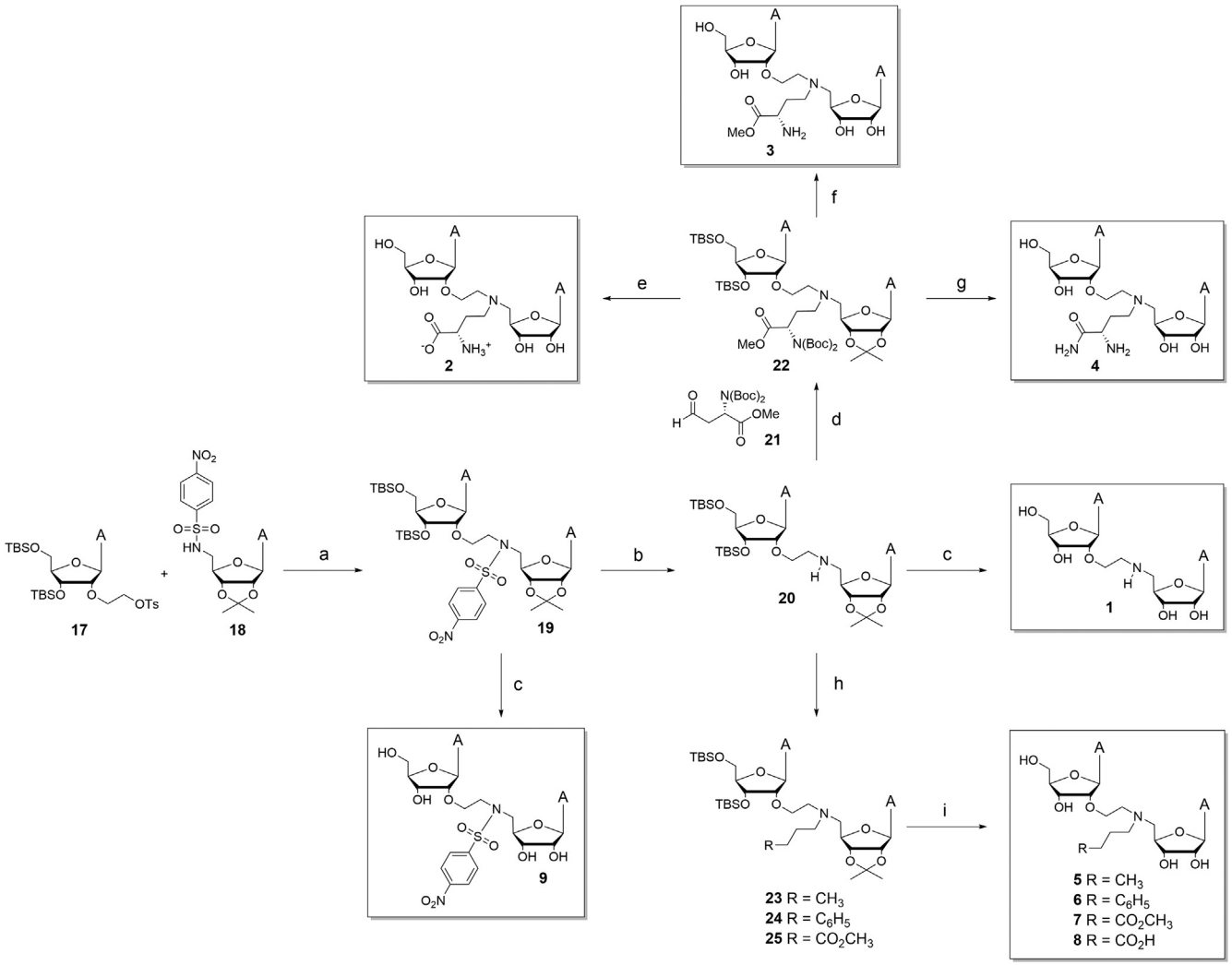

Scheme 2. Synthesis of dinucleosides **1**–**9**. (a) K_2CO_3, KI, DMF, 50 °C, 24 h, 74%; (b) PhSH, K_2CO_3, DMF, 25 °C, 2 h, 76%; (c) TFA/H_2O 8/2, 25 °C, 3 h, 76% for **1** and 34% for **9**; (d) (i) **21**, AcOH, CH_2Cl_2, 25 °C, 2 h, (ii) $NaBH(OAc)_3$, 25 °C, 2 h, 93%; (e) (i) TFA/H_2O 8/2, 25 °C, 3 h, (ii) 2 M aqueous solution LiOH, 25 °C, 0.5 h, 32%; (f) TFA/H_2O 8/2, 25 °C, 3 h, 35%; (g) (i) TFA/H_2O 8/2, 25 °C, 3 h, (ii) 7 M NH_3/MeOH, 30 °C, 24 h, 38%; (h) 1-bromobutane, DIEA, NMP, microwave 110 °C, 4 h, 47% for **23**; 1-bromo-3-phenylpropane, DIEA, NMP, microwave 110 °C, 4 h, 53% for **24**, methyl 4-bromobutyrate, DIEA, NMP, microwave 110 °C, 3.5 h, 58% for **25**; (i) (i) TFA/H_2O 8/2, 25 °C, 6 h, 72% for **5**; 3 h, 28% for **6**; 5.5 h, 60% for **7**; 5.5 h for **8**. (ii) 2 M aqueous solution LiOH, 0 °C, 0.5 h, 36% for **8**.

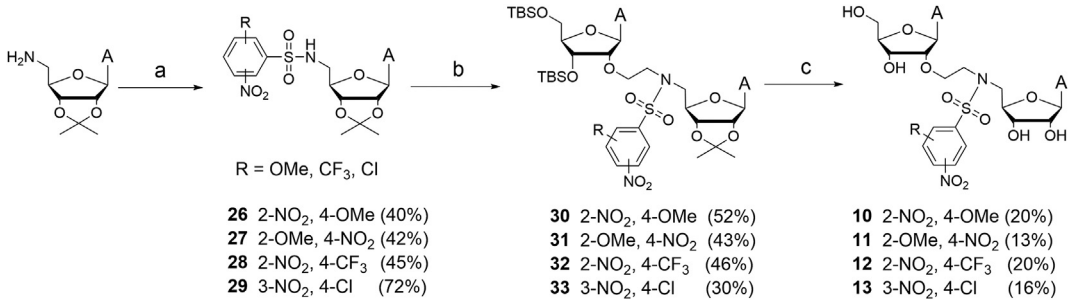

Scheme 3. Synthesis of dinucleosides **10**–**13**. (a) Ns-Cl, NEt_3, DMF, 25 °C, 3.5 h, 40–72%; (b) **17**, KI, K_2CO_3, DMF, 50 °C, 24 h, 43–52%; (c) TFA/H_2O 8/2, 25 °C, 3 h–5 h, 13–20%.

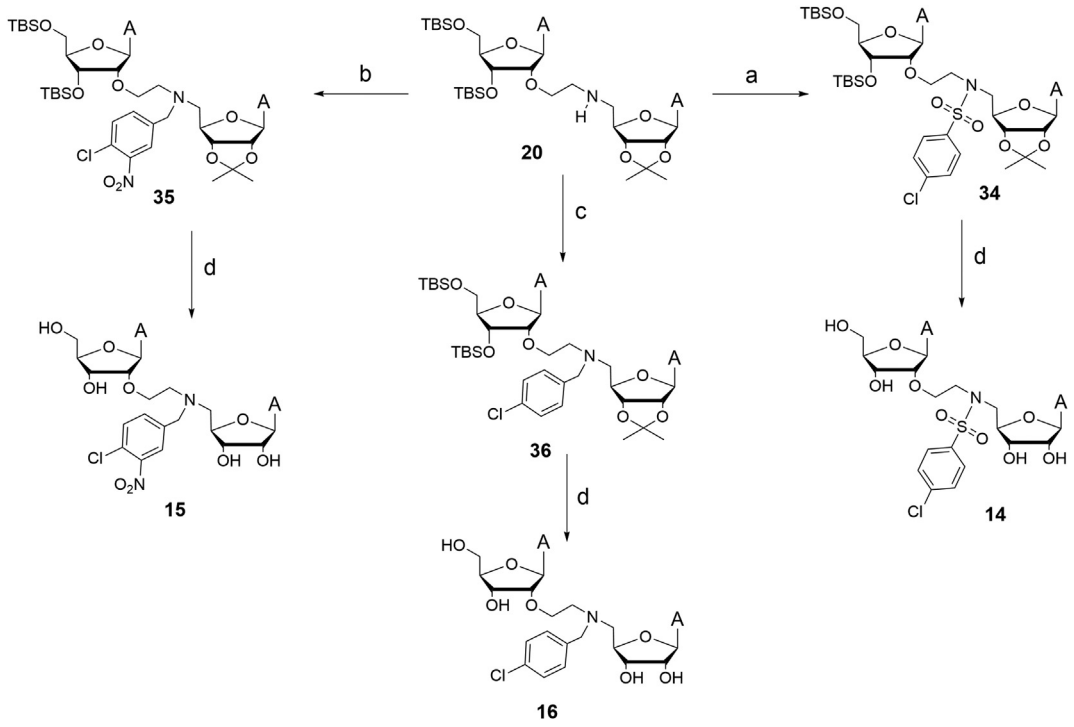

Scheme 4. Synthesis of dinucleosides **14**–**16**. (a) 4-chlorobenzenesulfonyl chloride, NEt_3, CH_2Cl_2, 0 °C, 3 h, 90%. (b) (i) 4-chloro-3-nitrobenzaldehyde, AcOH, DCE, 40 °C, 20 min; (ii) $NaBH(OAc)_3$, 40 °C, 16 h, 87%. (c) (i) 4-chlorobenzaldehyde, AcOH, DCE, 40 °C, 20 min. (ii) $NaBH(OAc)_3$, 40 °C, 16 h, 72%. (d) TFA/H_2O 8/2, 25 °C, 3 h, 48% for **14**; 6 h, 25% for **15**; 6 h, 37% for **16**.

2.2. Chemistry

The retrosynthetic analysis of the dinucleoside **1** structure suggested the coupling reaction between the tosyl derivative **17** previously described by us (Scheme 2) [14], and the readily accessible 5′-amino-2′,3′-isopropylidene adenosine [21]. The direct *N*-alkylation at room temperature did not afford the secondary amine in satisfactory yields and when increasing the temperature to enhance the reactivity of the primary amine, we noticed degradation of **17**. To circumvent the lack of reactivity of primary amines, a synthetic method using nitrobenzenesulfonamides (Ns-amides) as both a protecting and activating group has been developed by Fukuyama [22]. The main advantage of this nosyl strategy is that both alkylation and deprotection proceed under mild conditions. Recently, the 2-nitrobenzenesulfonamide has been used successfully to synthetize transition state analogs of DNA methylation based on the coupling of cytosine analogs to adenosine [15]. In the same way, we envisaged the coupling between **17** and the 5′-nosyl adenosine **18** to obtain the dinucleoside **1** (Scheme 2). The building block **18** was prepared in 74% yield by reacting 4-nitrobenzenesulfonyl chloride [22] that has a similar reactivity to 2-nitrobenzenesulfonyl chloride as used in Ref. [15], with 5′-amino-2′,3′-isopropylidene adenosine prepared upon published procedures [23]. *N*-alkylation of Ns-amide **18** with **17** in the presence of K_2CO_3 in DMF at room temperature did not afford the expected dinucleoside **19**, even at high temperature. Nevertheless, according to the literature [24], the addition of a catalytic amount of KI to the reaction mixture was beneficial to give **19** in 74% yield. Facile deprotection of **19** by treatment with a nucleophilic thiolate produced the desired secondary amine **20** in high yield. Removal of sugar protecting groups has been accomplished in acidic medium to give dinucleoside **1** in 76% yield. Likewise, the acidic treatment was applied to the intermediate Ns-amide **19** to afford the 4-nitrobenzenesulfonamide-containing dinucleoside **9** in 34% yield (Scheme 2).

Compounds **2**, **3** and **4** were obtained from key compound **20** *via* reductive amination of the aldehyde **21** that was prepared in three steps from L-aspartic acid following a published procedure [25].

Reductive amination was conducted in the presence of sodium triacetoxyborohydride and acetic acid [26]. The resulting fully protected dinucleoside **22** was isolated in high yield (93%). Then, sugar hydroxyls and amine were deprotected by TFA treatment and afforded methyl ester derivative **3**. Subsequent basic treatment with LiOH converted the methyl ester in carboxylic acid and dinucleoside **2** with α-amino acid chain similar to that of SAM was obtained. Finally, the SAM analogue **4** with an amide function instead of a carboxylic acid in α-amino acid chain was prepared from **22** upon a final treatment with 7 M methanolic ammonia solution. Dinucleosides **5**, **6** and **7** were rather synthesized through *N*-alkylation of **20** with 1-bromobutane, 1-bromo-3-phenylpropane or methyl-4-bromobutyrate, respectively, in *N*-methylmorpholine in the presence of diisopropylethylamine (DIEA) at 110 °C under microwave. These specific conditions were optimized for a successful synthesis of **23**, **24** and **25** with an average 50% yield. This moderate yield results from double *N*-alkylations (observed in mass spectrometry) and incomplete reactions. Increasing temperature of the reactions neither did drive the reaction to completion. Next, **23**, **24** and **25** were deprotected upon TFA treatment to obtain *N*-alkyl derivatives **5**, **6** and **7**, respectively. Subsequently, an additional basic treatment with 2 M LiOH was applied to **7** to convert the methyl ester moiety into the carboxylic acid-ended alkyl chain of compound **8**. The same synthetic route used for the preparation of nosyl-containing dinucleoside **9** was followed to synthesize compounds **10**–**13** with diverse Ns-amide moieties as analogs of the nosyl group (Scheme 3). The reaction of 5′-amino-2′,3′-isopropylidene adenosine [23] with four diversely substituted (OMe, CF_3, Cl) and commercially available nitrobenzenesulfonyl chloride reagents afforded the corresponding *N*-nosyl adenosines **26**–**29** with 40–72% yield [27–30]. Their subsequent coupling with **17** in the presence of K_2CO_3 and KI gave the corresponding dinucleosides **30**–**33** in moderate yields from 43 to 52%. A final TFA treatment provided the respective *N*-nosyl adenine dinucleosides **10**–**13** which were purified by reversed-phase chromatography (Yield 13–20%).

Scheme 4 depicts the synthesis of the adenine dinucleosides **14**–**16** from the intermediate NH-linked dinucleoside **20** (Scheme 2). The reaction of 4-chlorobenzenesulfonyl chloride with **20** in the presence of NEt_3 [31,32] followed by a TFA treatment yielded **14**. The treatment of **20** with 4-chloro-3-nitrobenzaldehyde or 4-chlorobenzaldehyde and sodium triacetoxyborohydride, followed by the removal of protective groups in acidic conditions resulted in dinucleosides **15** and **16**, respectively. It is noteworthy that this reductive amination conducted at 40 °C increased the yields to 71% and 81%, respectively.

2.3. RNA methyltransferase activity assays

Compounds **1**–**16** were tested for their ability to inhibit the methylation of the RNA cap structure. The inhibition induced by each compound (50 μM) was determined by a radioactive MTase assay (filter binding assay) which consists in measuring the [^{3}H] radiolabeled methyl transferred from the methyl donor SAM onto RNA substrate ($GpppAC_4$) synthetized by using T7 primase [33]. Compounds **1**–**16** designed as mimics of the transition state of RNA 2′-*O*-methylation were screened against several viral RNA 2′-*O*-MTases from SARS-CoV (nsp10/nsp16 complex), Zika, West-Nile, Dengue, Vaccinia (VP39) viruses. At the same time, the compounds were tested against human RNA N7-MTase (hRNMT) and selected viral N7-MTases such as SARS-CoV nsp14 and Vaccinia D1-D12 complex to evaluate their specificity (Table 1).

Unexpectedly, all the bisubstrate compounds were barely active against the 2′-*O* MTases of flaviviruses or coronavirus SARS-CoV. In contrast, most of the compounds displayed inhibition of N7-MTases. Dinucleoside **2** bearing the amino acid chain of the SAM showed some significant inhibition of both viral N7-MTases with a better activity on Vaccinia D1-D12 than on SARS-CoV nsp14. However, compound **2** also displayed a potent inhibition of hRNMT in the same range as the viral MTases displaying a lack of specificity against human and viral enzymes. The amino acid group of **2** seems essential for inhibition since compound **1** with a non-substituted NH linker weakly inhibited the three MTases. The replacement of the amino acid group with an α-amino-ester at the extremity in compound **3** is detrimental for the inhibitory activity. Interestingly, the dinucleoside **4** bearing an α-amino-amide specifically inhibited the viral protein Vaccinia D1-D12 complex whereas did not show any inhibition of SARS-CoV nsp14 or hRNMT. Replacing the amino acid chain by a more hydrophobic butyl or phenylpropyl chain in dinucleosides **5** and **6**, respectively, we aimed at favoring the Van der Waals interactions in hydrophobic pockets of the protein. Only compound **6** showed a moderate but specific inhibition of SARS-CoV nsp14. The removal of the NH_2 of the amino acid chain of the broader spectrum inhibitor **2** with an ester-ended butyl chain in compound **7** or with an acid-ended butyl chain in **8** induced weaker but more specific inhibitions of Vaccinia D1-D12 MTase and SARS-CoV nsp14. In the synthetic pathway of dinucleoside **1**, the intermediate **19** bearing a 4-Ns-amide group was prepared. In view of the valuable properties of such motif in some antiviral or anticancer drugs [19,20] it seemed interesting to us to obtain dinucleoside **9** by simple acidic deprotection of **19**. Of special interest, compound **9** showed a good and specific inhibition on SARS-CoV nsp14 confirming that the nosyl group contributes to the inhibitory activity with specificity. Then, we modulated the initial nosyl moiety with the nitro group in “para” position by introducing diverse hydrophobic substituents (Cl, OMe, CF_3) at different positions on the phenyl ring and/or by varying the position of the nitro group in compounds **10**–**13**. The addition of such substituents aimed at increasing the interactions with proteins. Like **9**, the four dinucleosides **10**–**13** maintained a high inhibitory activity on SARS-CoV nsp14. The role of the nitro group on the phenyl ring was

Table 1
Screening for inhibitory activity of sinefungin and compounds **1**–**16** at 50 μM on N7-MTases.

Compounds	Percentage of inhibition at 50 μM (%)[a]		
	SARS-CoV nsp14	Vaccinia virus D1-D12	hRNMT
Sinefungin	98.3 ± 0.2	99.8 ± 0.1	99.8 ± 0.2
1	31.0 ± 6.8	20.3 ± 0.8	35.2 ± 4.9
2	72.0 ± 1.2	85.8 ± 2.5	77.4 ± 1.2
3	30.6 ± 9.3	32.1 ± 2.4	33.2 ± 4.3
4	13.1 ± 13.3	53.2 ± 2.6	12.2 ± 2.1
5	n.i	n.i	27.5 ± 6.6
6	38.4 ± 11.7	11.6 ± 7.1	23.1 ± 9.7
7	n.i	69.2 ± 1.9	32.8 ± 16.1
8	43.0 ± 4.0	n.i	n.i
9	88.6 ± 1.3	49.8 ± 3.2	66.0 ± 6.1
10	96.6 ± 0.9	4.6 ± 0.3	31.8 ± 3.3
11	47.6 ± 2.8	5.3 ± 4.3	44.2 ± 8.5
12	94.6 ± 1.1	10.1 ± 5.5	23.3 ± 3.6
13	97.2 ± 2.7	2.8 ± 0.8	33.9 ± 3.3
14	96.2 ± 1.5	19.7 ± 3.8	20.2 ± 9.4
15	94.0 ± 1.1	4.3 ± 3.9	n.i
16	75.9 ± 2.5	4.5 ± 15.1	14.7 ± 1.3

[a]Values are the mean of three independent experiments. The MTase activity was measured using a filter binding assay. Assays were carried out in reaction mixture [40 mM Tris-HCl (pH 8.0), 1 mM DTT, 1 mM $MgCl_2$, 2 μM SAM and 0.1 μM ^{3}H-SAM] in the presence of 0.7 μM $GpppAC_4$ synthetic RNA and incubated at 30 °C. SARS-CoV nsp14 (50 nM), vaccinia virus capping enzyme (D1-D12) (41 U), human RNA N7 MTase (hRNMT) (50 nM). Compounds were previously dissolved in 100% DMSO. n.i: no inhibition detected at 50 μM.

Table 2
Comparison of IC_{50} values of 10 most active compounds on SARS-CoV nsp14 and human RNMT activities.

Compounds	SARS-CoV nsp14 IC_{50}[a] (μM)	hRNMT IC_{50} (μM)
Sinefungin[b]	0.36	<0.05
2	40.6 ± 3.2	10.9 ± 1.0
6	55.5 ± 5.1	>500
9	2.6 ± 0.2	>500
10	3.9 ± 0.4	>500
11	70.4 ± 4.9	169.3 ± 30.4
12	5.7 ± 0.5	275.9 ± 28.7
13	0.6 ± 0.1	247.5 ± 14.9
14	1.5 ± 0.1	n.d
15	2.4 ± 0.2	n.i
16	9.9 ± 0.9	n.d

[a] Concentration inhibiting MTase activity by 50%; mean value from three independent experiments.
[b] values from the literature [11]. The MTase activity for IC_{50} determinations was measured using a filter binding assay as described above. n.i: no inhibition detected at 50 μM; n.d: not determined due to inhibition lower than 50% at 50 μM.

demonstrated by removing it in dinucleoside **14** bearing solely one chlorine atom in "para" position, thus the inhibitory effect was slightly decreased. These data indicated the importance of the hydrophobic Cl in "para" position. Finally, the resulting decreased inhibition when the sulfone moiety of **14** was replaced by a methylene group in compounds **15** and **16** stressed the importance of the *N*-arylsulfonylbenzene motif in the dinucleoside structure to maintain an effective inhibition.

2.4. Dose-response testing of selected compounds against SARS-CoV nsp14 and hRNMT

To confirm the observed inhibition of some adenine dinucleosides against SARS-CoV nsp14 N7-MTase, we further tested 10 compounds in a dose-response assay (Table 2, Supporting Information Fig. S2). The selection of these compounds was based on their percentage inhibition higher than 50% against SARS-CoV nsp14 (Table 1). After pre-incubation with increasing concentrations of dinucleosides, the MTase activity was measured by FBA. The IC_{50} of compounds, deduced from Hill slope equation (Y = 100/(1+((X/IC_{50})^Hillslope) curve-fitting, ranged from 0.6 μM to 70.4 μM on SARS-CoV nsp14 and 10.9 μM to > 500 μM on hRNMT activity. Among all the potential inhibitors, three compounds **2**, **6** and **11** showed the lowest inhibitory activity on SARS-CoV nsp14 with IC_{50} > 40 μM, the others have IC_{50} values in the micromolar range except **13** that showed an IC_{50} value in the submicromolar range. The potency of the derivative **13** to inhibit SARS-CoV nsp14 was comparable to the broad spectrum inhibitor sinefungin. However, it is noteworthy that compound **13** specifically inhibits the N7-MTase of SARS-CoV with a high 413-fold of specificity in dose-response testing whereas sinefungin is also active against hRNMT [11]. Remarkably **13** bearing a chlorine atom in "para" position and a nitro group in "meta" position displayed the best inhibition which was 6.5–9.5 fold more potent than the derivatives **10** and **12**, respectively that contain the nitro in "ortho" position and a lipophilic group CF_3 or MeO in "para" position. The comparison of IC_{50} values of **14** and **13** indicates that the addition of a nitro group in the phenyl ring increased the inhibitory activity by 2.5 fold in **13**. These results confirm that the chlorine atom in "para" position and the presence of a nitro group seem crucial for submicromolar SARS-CoV nsp14 inhibitory activity.

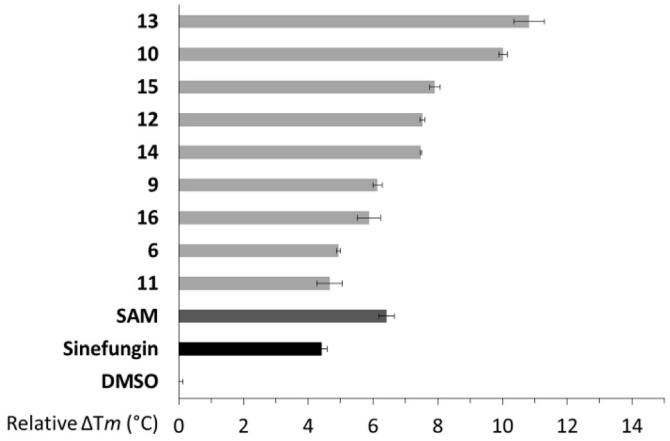

Fig. 2. Thermal shifts (ΔTm) of SARS-CoV nsp14 in the absence or presence of SAM, sinefungin and 9 dinucleoside inhibitors **6** and **9**–**16**. Thermal stability of SARS-CoV nsp14 upon ligand binding was monitored by differential scanning fluorimetry. Assays were carried out in reaction mixture [20 mM HEPES (pH 7.5), 150 mM NaCl, 1x SYPRO orange dye] in the presence of 5 μM SARS-CoV nsp14 protein and 1 mM compound previously dissolved in 100% DMSO. The bars and error bars correspond to the mean values from three independent measurements and their s.d.'s, respectively.

2.5. Thermal shift DSF assays for SARS-CoV nsp14

SARS-CoV nsp14-inhibitor interactions were further investigated by monitoring the thermal stability of the protein using differential scanning fluorimetry (DSF) (Supporting Information, Fig. S3) [34]. The change in thermal stability of SARS-CoV nsp14 was monitored in response to binding of the natural cofactor substrate SAM, sinefungin and the 9 most active and specific compounds **6** and **9**–**16** with IC_{50} < 100 μM. As expected, SARS-CoV nsp14 displayed an increased melting temperature (T_m) value with SAM (+6.5 °C) and sinefungin (+4.4 °C) whose structure only differs by a C–NH_2 in place of S^+-CH_3 group in SAM (Fig. 2). The binding experiments with the bisubstrate inhibitors showed that all dinucleosides stabilized the SARS-CoV nsp14 protein (T_m > 40 °C) with a T_m shift from +4.6 °C to +10.8 °C (Supporting Information, Table S1). Eight of the 9 examined compounds increased the stability of SARS-CoV nsp14 more efficiently than the well-known inhibitor sinefungin. More interestingly, T_m values for SARS-CoV nsp14 were larger in the presence of five compounds **10** and **12**–**15** than with the natural enzyme substrate SAM, suggesting strong protein-inhibitor interactions. Remarkably, the highest T_m was observed with the most efficient inhibitor **13** (IC_{50} 0.6 ± 0.1 μM) that stabilizes SARS-CoV nsp14 against thermal denaturation with a ΔT_m +10.8 °C and exhibits notable binding affinity (apparent K_D 1.3 ± 0.87 μM), as deduced from TSA performed with increasing concentration of compound **13**. This demonstrates a favorable interaction and highlights the inhibitor potential of compound **13**. The T_m comparison of compounds **16**, **15** and **13** showed a respective increase in SARS-CoV nsp14 stability, settling the importance of the sulfone group, the Cl and NO_2 substituents in protein binding with **13**. Thus the *N*-(4-Cl-3-NO_2-phenylsulfonamide) moiety is notably preferred for optimal SARS-CoV nsp14 interactions. Another highlight is the thermal shift (+5.4 °C) for SARS-CoV nsp14 observed in the presence of compound **10** compared to **11**, both only differ by the position of OCH_3 and NO_2 substituents in the phenyl ring. A higher stability and inhibition of SARS-CoV nsp14 was observed when the OCH_3 group is in "para" position in dinucleoside **10**.

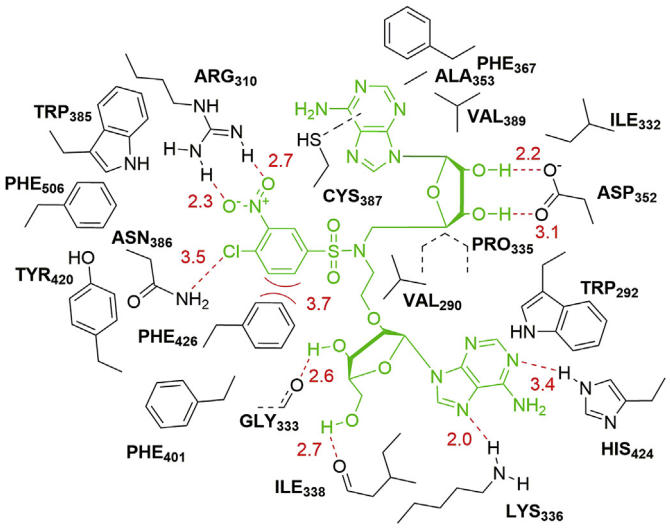

Fig. 3. Modeling results in the SAM binding pocket of SARS-CoV nsp14 (PDB ID: 5C8T, resolution 3.2 Å). (A) Amino acids surrounding dinucleoside **13**. Hydrogen and halogen bonds are indicated by red dashes. π-π stacking interaction is indicated by red curve. Distances are given in Å. (For interpretation of the references to color in this figure legend, the reader is referred to the Web version of this article.)

2.6. Molecular docking studies of SARS-CoV nsp14 in complex with dinucleoside *13*

To address the molecular bases of N7-MTase nsp14 inhibition by the dinucleosides, we performed computational docking studies of the best inhibitor **13** using Autodock Vina. The docking was based on the SARS-CoV nsp14-nsp10 complex structure solved in presence of SAM [35]. SARS-CoV nsp14 is a bifunctional enzyme carrying RNA cap guanine N7-MTase at the C-terminal domain for mRNA capping (which is not influenced by nsp10) and 3′-5′-exoribonuclease at the N-terminal domain for proofreading. The N7-MTase domain exhibits an original fold and the methyl receptor cap RNA (GpppA-RNA) and SAM bind in proximity in a highly constricted pocket to achieve methyltransfer. The compound **13** was modeled in the SAM binding pocket of the SARS-CoV nsp14 structure (PDB ID: 5C8T [35] & PDB ID: 5NFY [36]). At first sight, the overlay of the *N*-adenosine of **13** with the adenosine of SAM bounded structure is suitable (Supporting Information, Fig. S4). More interestingly, the nitrobenzenesulfonamide core of **13** binds into a SARS-CoV nsp14 well known binding site formed by Trp385, Phe401, Tyr420, Phe426 and Phe506 (Fig. 3, Supporting Information, Fig. S5) [35]. Naturally, the side chains of these amino acids enclose the nucleobase guanine of the cap structure. In this cap-binding site, Phe426 was shown to have the largest influence on the N7-MTase activity, and F426A mutation reduced MTase activity by 50%. With **13**, the orientation of the Phe426 residue all around the nitrobenzenesulfonamide leads to the formation of π-π stacking interactions. In addition, there are other hydrophobic interactions between the phenylsulfonamide moiety and aromatic residues of the binding site. All these interactions may explain the strong inhibition observed with phenyl-containing compounds, notably compounds **13**–**15**. Moreover, Asn386 is located in proximity to the methylation site and forms two hydrogen bonds with the guanine moiety favoring its right orientation for methylation. Here, fixed on the nitrobenzenesulfonamide core of **13**, the chlorine atom forms a halogen bond with Asn386 (Fig. 4) [37]. The formation of a double hydrogen bond interaction was observed between the nitro group and Arg310 that normally interacts with the second phosphate group of the triphosphate bond in the cap structure. The docking also suggests that the sulfone group of **13** avoids flexibility of the *N*-nosyl substituent, thus increasing its orientation into the pocket. This constraint may explain the difference in activity (IC_{50}) and stabilizing effect (T_m) between compounds **13** and **15** that contains a methylene group instead of the sulfone. Finally, the common element of all dinucleosides is an adenosine linked to a *N*-adenosine by the 2′*O* position. Its contribution is well defined by the formation of intermolecular hydrogen bonds between the adenosine and Gly333 (3′OH), Ile338 (5′OH), Lys336 (N7) and His424 (N1) residues (Fig. 4). All the major interactions maintain **13** in a suitable orientation in the binding site in place of the natural substrate GpppA-RNA. The docking model of **13** is consistent with our inhibition experimental data and high thermal stability of SARS-CoV nsp14 in the presence of these compounds.

3. Conclusion

We synthesized 16 adenine dinucleosides which were designed as bisubstrate SAM analogs to mimic the transition state of 2′-*O*-methylation of the cap RNA. Both adenosines were connected by various NH or N-substituted linkers between the 2′-*O*-position of the adenosine representing the 5′-end nucleoside of mRNA and the 5′-position of the adenosine mimicking the SAM cofactor in the methylation reaction. None of these bisubstrate SAM analogs were found to inhibit 2′-*O* MTases of several flaviviruses, coronavirus or pox-virus at 200 μM. Conversely, six of them inhibited SARS-CoV nsp14 N7-MTase in micromolar range concentration and one in submicromolar range. Additionally, we also observed that these compounds barely inhibit the human RNA N7 MTase, an important feature given that the lack of antiviral specificity represents a common issue in coronavirus antiviral discovery. Indeed, the structural homology between viral and cellular MTases often impairs the discovery of specific inhibitors for CoV N7-MTase. Nevertheless, our work did identify one dinucleoside (**13**) bearing a 4-chloro-3-nitrobenzenesulfonamide moiety in the *N*-linker between both adenosines, that blocks the activity of SARS-CoV nsp14 at the submicromolar concentration in the same range than sinefungin but with a significant specificity. Thermal shift assays and molecular modeling indicate that the inhibitory activity is likely due to the binding of **13** to both SAM and mRNA binding pockets of nsp14. It is quite interesting to note that all residues of SARS-CoV nsp14 involved in the binding of **13** are fully conserved in the SARS-CoV-2 nsp14 protein (Fig. S1, Supporting Information). Indeed, the genome sequence of SARS-CoV-2 nsp14 exhibits about 95% sequence similarity with SARS-CoV nsp14 [38]. The lead compound **13** and the most potent derivatives will serve as starting building blocks for the development of SARS-CoV-2 nsp14 inhibitors.

4. Experimental section

4.1. Chemistry

4.1.1. General procedures

All dry solvents and reagents were purchased from commercial suppliers and were used without further purification. DIEA was distilled over calcium hydride. Thin-layer chromatography (TLC) analyses were carried out on silica plate 60 F_{254}. Purifications by column chromatography were performed using Biotage Isolera 1 system with FlashPure cartridges (Buchi). NMR experiments were recorded on Bruker 400, 500 or 600 MHz spectrometers at 20 °C. HRMS analyses were obtained with electrospray ionization (ESI) in positive mode on a Q-TOF Micromass spectrometer. Analytical HPLC was performed on a UHPLC Thermoscientific Ultimate 3000 system equipped with a LPG-3400RS pump, a DAD 3000 detector

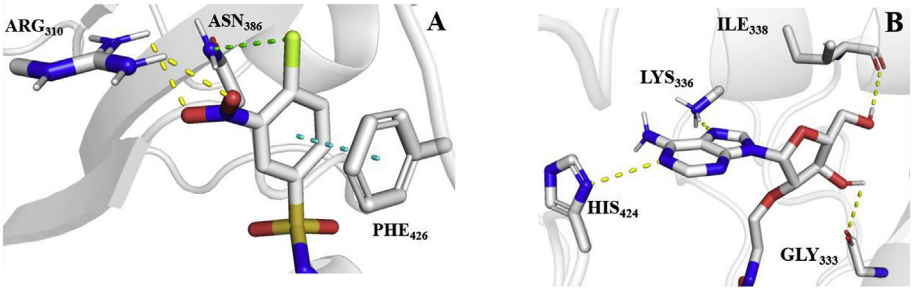

Fig. 4. Modeling results in the SAM binding pocket of SARS-CoV nsp14 (PDB ID: 5C8T, resolution 3.2 Å). (A) Contribution of the nitrobenzenesulfonamide core of **13**. (B) Contribution of the 2′O linked adenosine of all dinucleosides, including **13**. Hydrogen bonds (yellow), halogen bond (green) and π-π stacking interaction (cyan) are represented. (Atoms not involved in protein-ligand interaction are not represented for clarity purpose). (For interpretation of the references to color in this figure legend, the reader is referred to the Web version of this article.)

and an WPS-3000TBRS Autosampler, Column Oven TCC-3000SD. Dinucleosides **1**–**16** were analyzed by RP-HPLC on a Column Nucleodur C_{18} ec 100-3, 4.6 × 75 mm (Macherey Nagel) at 30 °C. The following HPLC solvent systems were used: 1% CH_3CN in 12.5 mM TEAAc (buffer A), 80% CH_3CN in 12.5 mM TEEAc (buffer B). Flow rate was 1 mL/min. UV detection was performed at 260 nm. Lyophilized compounds **1**–**16** were stored at −20 °C for several months without any degradation.

4.1.2. General method A for the synthesis of compounds 18, 26, 27 and 29

To a solution of 5′-amino-2′,3′-isopropylidene adenosine in anhydrous DMF (conc. 0.2 M) was added Et_3N (2.00 eq) and the corresponding nitrobenzenesufonyl chloride (1.50 eq) at 0 °C. The reaction mixture was stirred for 4 h at room temperature under argon then was diluted with AcOEt and brine. The aqueous layer was extracted with AcOEt and the combined organic extracts were washed with brine, dried over Na_2SO_4 and concentrated under vacuum. The precipitate was washed with Et_2O and DCM to give the desired compound as a colored solid.

4.1.3. N-{[(4R,6R)-6-(6-amino-9H-purin-9-yl)-2,2-dimethyl-tetrahydro-2H-furo[3,4-d] [1,3]dioxol-4-yl]methyl}-4-nitrobenzene-1-sulfonamide (18)

Following **method A** with 5′-amino-2′,3′-isopropylidene adenosine (2.21 g, 7.22 mmol, 1.00 eq) and 4-nitrobenzenesufonyl chloride, **18** (2.64 g, 74%) was obtained as a beige solid. R_f 0.50 (8:92 MeOH/DCM). ^{1}H NMR (600 MHz, DMSO-d_6) δ 8.55 (t, J = 5.8 Hz, 1H), 8.33–8.27 (m, 2H), 8.26 (s, 1H), 8.13 (s, 1H), 7.96–7.88 (m, 2H), 7.37 (br. s, 2H), 6.09 (d, J = 2.8 Hz, 1H), 5.32 (dd, J = 6.3 Hz, 2.9 Hz, 1H), 4.89 (dd, J = 6.3 Hz, 3.0 Hz, 1H), 4.16 (td, J = 5.9 Hz, 3.0 Hz, 1H), 3.24–3.10 (m, 2H), 1.50 (s, 3H), 1.27 (s, 3H). ^{13}C NMR (600 MHz, DMSO-d_6) δ 156.3, 152.7, 149.5, 148.4, 146.0, 140.2, 128.0, 124.5, 119.3, 113.6, 89.4, 84.4, 83.0, 81.6, 44.6, 27.0, 25.2. HRMS (ESI+): m/z calcd for $C_{19}H_{22}N_7O_7S$ $[M+H]^+$: 492.1301, Found 492.1311.

4.1.4. General method B for the synthesis of compounds 19, 30-33

To a solution of **18** or **26**–**29** in anhydrous DMF (conc. 0.13 M) was successively added **17** (1.10 eq), KI (0.30 eq) and K_2CO_3 (3.00 eq). After stirring for 24 h at 50 °C under argon, the reaction was diluted in AcOEt and water. The aqueous layer was extracted with AcOEt and the combined organic extracts were washed with brine, dried over Na_2SO_4 and concentrated under vacuum. The residue was purified by flash column chromatography (silica gel, linear gradient 0–8% MeOH in DCM) to give the desired compound as colored solid.

4.1.5. N-{[(4R,6R)-6-(6-amino-9H-purin-9-yl)-2,2-dimethyl-tetrahydro-2H-furo[3,4-d] [1,3]dioxol-4-yl]methyl}-N-(2-{[(2R,5R)-2-(6-amino-9H-purin-9-yl)-4-[(tert-butyldimethylsilyl)oxy]-5-{[(tert-butyldimethylsilyl)oxy]methyl}oxolan-3-yl]oxy}ethyl)-4-nitrobenzene-1-sulfonamide (19)

Following **method B** using **18** (290 mg, 0.59 mmol, 1.00 eq), **19** (450 mg, 74%) was obtained as a pale yellow solid. R_f 0.60 (10:90 MeOH/DCM). ^{1}H NMR (600 MHz, $CDCl_3$) δ 8.30 (2s, 2H), 8.14 (s, 1H), 8.03–7.98 (m, 2H), 7.74 (s, 1H), 7.70–7.66 (m, 2H), 6.11–5.93 (m, 5H), 5.89 (d, J = 1.9 Hz, 1H), 5.35 (dd, J = 6.4 Hz, J = 1.9 Hz, 1H), 5.04 (dd, J = 6.4 Hz, J = 3.8 Hz, 1H), 4.51 (dd, J = 6.1 Hz, J = 4.6 Hz, 1H), 4.43 (dt, J = 8.5 Hz, J = 4.2 Hz, 1H), 4.22 (dd, J = 4.7 Hz, J = 3.2 Hz, 1H), 4.05 (dt, J = 5.9 Hz, J = 3.0 Hz, 1H), 3.99 (dd, J = 11.5 Hz, J = 3.5 Hz, 1H), 3.85–3.41 (m, 7H), 1.57 (s, 3H), 1.35 (s, 3H), 0.92 (s, 9H), 0.91 (s, 9H), 0.14–0.04 (m, 12H). ^{13}C NMR (150 MHz, $CDCl_3$) δ 155.8, 155.5, 153.2, 153.0, 149.7, 149.5, 148.9, 145.4, 140.2, 139.5, 128.4, 123.8, 120.5, 120.2, 114.7, 90.7, 87.3, 85.0, 84.5, 84.2, 82.8, 82.6, 69.7, 69.6, 61.5, 50.7, 47.7, 27.3, 26.2, 25.9, 25.4, 18.6, 18.2, −4.4, −4.7, −5.2, −5.3. HRMS (ESI+): m/z calcd for $C_{43}H_{65}N_{12}O_{11}SSi_2$ $[M+H]^+$: 1013.4155, found: 1013.4155.

4.1.6. 9-[(2R,5R)-3-[2-({[(4R,6R)-6-(6-amino-9H-purin-9-yl)-2,2-dimethyl-tetrahydro-2H-furo[3,4-d] [1,3]dioxol-4-yl]methyl}amino) ethoxy]-4-[(tert-butyldimethylsilyl)oxy]-5-{[(tert-butyldimethylsilyl)oxy]methyl}oxolan-2-yl]-9H-purin-6-amine (20)

To a solution of **19** (210 mg, 0.20 mmol, 1.00 eq) in anhydrous DMF (10 mL) was added K_2CO_3 (85 mg, 0.61 mmol, 3.00 eq) and thiophenol (11 μL, 1.14 mmol, 5.70 eq). After stirring for 2 h at room temperature under argon, the reaction mixture was diluted with DCM (20 mL) and washed with 1 M aqueous NaOH solution (10 mL). The aqueous layer was extracted with DCM (3 × 20 mL) and the combined organic extracts were washed with brine, dried over Na_2SO_4 and concentrated under vacuum. The residue was purified by flash column chromatography (silica gel, linear gradient 0–15% MeOH in DCM) as the eluent to give **20** (129 mg, 76%) as a white solid. R_f 0.31 (8:92 MeOH/DCM). ^{1}H NMR (500 MHz, $CDCl_3$) δ 8.32 (s, 1H), 8.31 (s, 1H), 8.17 (s, 1H), 7.93 (s, 1H), 6.17–6.06 (m, 5H), 6.03 (d, J = 2.9 Hz, 1H), 5.39 (dd, J = 6.5 Hz, J = 3.0 Hz, 1H), 4.99–4.92 (m, 1H), 4.51–4.45 (m, 1H), 4.33–4.25 (m, 2H), 4.08 (dt, J = 5.6 Hz, J = 3.2 Hz, 1H), 3.98 (dd, J = 11.5 Hz, J = 3.6 Hz, 1H), 3.75 (dd, J = 11.6 Hz, J = 2.8 Hz, 1H), 3.71–3.63 (m, 2H), 2.95–2.69 (m, 4H), 1.61 (s, 3H), 1.37 (s, 3H), 0.92 (s, 9H), 0.88 (s, 9H), 0.13–0.04 (m, 12H). ^{13}C NMR (125 MHz, $CDCl_3$) δ 155.8, 155.7, 153.3, 153.1, 149.7, 149.6, 139.8, 139.4, 120.5, 120.3, 114.8, 90.7, 87.2, 85.8, 85.1, 83.9, 82.6, 82.4, 70.3, 70.13, 62.0, 51.5, 49.5, 27.4, 26.2, 25.8, 18.6, 18.2, −4.5, −4.8, −5.2, −5.3. HRMS (ESI+): m/z calcd for $C_{37}H_{62}N_{11}O_7Si_2$ $[M+H]^+$: 828.4372, found: 828.4371.

4.1.7. General method C for the synthesis of compounds 1, 3, 5–7, 9, 10-16

The synthesis intermediate was treated at room temperature with TFA in water (8/2, conc. 0.14 M). After stirring for 3–6 h until completion of reaction (TLC DCM/MeOH), solvents were removed and the residue was coevaporated three times with 7 M NH_3 in MeOH. The residue was purified by flash column chromatography on a reversed-phase silica gel column C_{18} (4 g, 40 μm) with a linear gradient of acetonitrile in TEAAc buffer 50 mM, pH 7. The fractions containing the pure compound were pooled, concentrated and lyophilized with water/dioxane to give desired compound as a powder.

4.1.8. (2R,5R)-2-(6-amino-9H-purin-9-yl)-5-{[(2-{[(2R,5R)-2-(6-amino-9H-purin-9-yl)-4-hydroxy-5-(hydroxymethyl)oxolan-3-yl]oxy}ethyl)amino]methyl}oxolane-3,4-diol (1)

Following **method C** with **20** (117 mg, 0.14 mmol, 1.00 eq) and a 0–25% linear gradient of acetonitrile in TEAAc buffer 50 mM, pH 7 for purification, **1** (60 mg, 76%) was obtained as a white powder with 99% purity determined by HPLC analysis at 260 nm. ^{1}H NMR (600 MHz, DMSO-d_6) δ 8.38 (s, 1H), 8.34 (s, 1H), 8.15 (s, 1H), 8.14 (s, 1H), 7.36 (br.s, 2H), 7.29 (br. s, 2H), 5.97 (d, J = 6.4 Hz, 1H), 5.85 (d, J = 5.9 Hz, 1H), 5.58–4.98 (m, 4H), 4.70–4.63 (m, 1H), 4.52 (dd, J = 6.4 Hz, J = 4.7 Hz, 1H), 4.33 (dd, J = 4.7 Hz, J = 2.6 Hz, 1H), 4.12 (dd, J = 5.2 Hz, J = 3.8 Hz, 1H), 4.02–3.93 (m, 2H), 3.70–3.48 (m, 4H), 2.86–2.58 (m, 4H). ^{13}C NMR (150 MHz, DMSO-d_6) δ 156.2, 156.1, 152.6, 152.5, 149.4, 149.0, 140.1, 139.9, 119.4, 119.3, 87.6, 86.3 (2C), 83.7, 81.5, 72.8, 71.5, 69.5, 69.1, 61.7, 51.2, 49.0. HRMS (ESI+): m/z calcd for $C_{22}H_{30}N_{11}O_7$ $[M+H]^+$: 560.23242, found: 560.23188.

4.1.9. Methyl (2S)-4-({[(4R,6R)-6-(6-amino-9H-purin-9-yl)-2,2-dimethyl-tetrahydro-2H-furo[3,4-d] [1,3]dioxol-4-yl]methyl}(2-{[(2R,5R)-2-(6-amino-9H-purin-9-yl)-4-[(tert-butyldimethylsilyl)oxy]-5-{[(tert-butyldimethylsilyl)oxy]methyl}oxolan-3-yl]oxy}ethyl)amino)-2-{bis[(tert-butoxy)carbonyl]amino}butanoate (22)

To a solution of **20** (250 mg, 0.30 mmol, 1.00 eq) in anhydrous DCM (9 mL) was added aldehyde **21** (120 mg, 0.36 mmol, 1.20 eq) in anhydrous DCM (9 mL) and acetic acid (20 μL, 0.36 mmol, 1.20 eq). After stirring for 20 min at room temperature under argon, sodium triacetoxyborohydride (96 mg, 0.45 mmol, 1.5 eq) was added. After stirring for 2.5 h, the reaction mixture was diluted with DCM (30 mL) and washed with saturated aqueous $NaHCO_3$ (30 mL). The aqueous layer was extracted with DCM (3 × 30 mL) and the combined organic extracts were washed with brine, dried over Na_2SO_4 and concentrated under vacuum. The residue was purified by flash column chromatography (silica gel, linear gradient 0–8% MeOH in DCM) to give **22** (321 mg, 93%) as a white solid. R_f 0.71 (MeOH/DCM 5:95). ^{1}H NMR (600 MHz, $CDCl_3$) δ 8.33 (s, 1H), 8.30 (s, 1H), 8.17 (s, 1H), 7.93 (s, 1H), 6.09 (d, J = 3.3 Hz, 1H), 6.01 (d, J = 2.4 Hz, 1H), 5.97 (m, 4H), 5.42 (dd, J = 6.5 Hz, J = 2.4 Hz, 1H), 4.93–4.86 (m, 2H), 4.54–4.49 (m, 1H), 4.33 (td, J = 6.8 Hz, J = 3.3 Hz, 1H), 4.29–4.24 (m, 1H), 4.08 (dt, J = 6.2 Hz, J = 3.2 Hz, 1H), 3.99 (dd, J = 11.5 Hz, J = 3.7 Hz, 1H), 3.78–3.63 (m, 6H), 2.84–2.74 (m, 3H), 2.71–2.51 (m, 3H), 2.33–2.23 (m, 1H), 1.91–1.82 (m, 1H), 1.58 (s, 3H), 1.46 (s, 18H), 1.36 (s, 3H), 0.91 (s, 9H), 0.90 (s, 9H), 0.10–0.05 (m, 12H). ^{13}C NMR (125 MHz, $CDCl_3$) δ 171.6, 155.8, 155.7, 153.3, 153.2, 152.3, 149.7, 149.5, 140.1, 139.8, 120.5, 120.4, 114.5, 91.1, 87.4, 85.45, 84.8, 84.1, 83.3, 83.3, 82.5, 69.9, 69.1, 61.9, 56.3, 56.3, 53.7, 52.4, 52.1, 28.1, 28.1, 27.3, 26.2, 26.0, 25.6, 18.7, 18.3, −4.3, −4.6, −5.2, −5.2. HRMS (ESI+): m/z calcd for $C_{52}H_{87}N_{12}O_{13}Si_2$ $[M+H]^+$: 1143.6049, found: 1143.6043.

4.1.10. (2S)-4-({[(2R,5R)-5-(6-amino-9H-purin-9-yl)-3,4-dihydroxyoxolan-2-yl]methyl}(2-{[(2R,5R)-2-(6-amino-9H-purin-9-yl)-4-hydroxy-5-(hydroxymethyl)oxolan-3-yl]oxy}ethyl)amino)-2-azaniumylbutanoate (2)

Compound **22** (86 mg, 75.3 μmol, 1.00 eq) was treated at room temperature with TFA (830 μL) in water (210 μL). After stirring for 3 h, solvents were removed under vacuum. The residue was dissolved in water (0.5 mL) and 2 M aqueous LiOH solution (4 mL) was added. After stirring at 0 °C for 30 min, pH ≈ 3 or 4 was adjusted by addition of 1 M aqueous HCl solution. The solvent was removed under vacuum and the residue was purified by flash column chromatography on a reversed-phase silica gel column C_{18} (4 g, 40 μm) with a 0–15% linear gradient of acetonitrile in TEAAc buffer 50 mM, pH 7. The fractions containing the pure compound were pooled, concentrated and lyophilized with water to give **2** (16 mg, 32%) as a white powder with 99% purity determined by HPLC analysis at 260 nm. ^{1}H NMR (600 MHz, D_2O) δ 8.11 (s, 1H), 8.05 (s, 1H), 7.98 (s, 1H), 7.86 (s, 1H), 5.89 (d, J = 2.5 Hz, 1H), 5.77 (d, J = 3.3 Hz, 1H), 4.51–4.47 (m, 2H), 4.36 (dd, J = 5.1 Hz, J = 3.4 Hz, 1H), 4.34–4.29 (m, 1H), 4.14–4.08 (m, 2H), 3.97 (td, J = 10.6 Hz, J = 2.4 Hz, 1H), 3.89–3.80 (m, 3H), 3.71 (dd, J = 13.0, J = 3.4 Hz, 1H), 3.15–3.04 (m, 2H), 3.03–2.81 (m, 2H), 2.76 (d, J = 14.2 Hz, 1H), 2.58 (d, J = 13.8 Hz, 1H), 2.14–1.99 (m, 2H). ^{13}C NMR (150 MHz, D_2O) δ 174.5, 154.9 (2C) 152.5, 152.2, 147.7, 147.5, 139.3, 138.5, 118.5, 118.2, 89.0, 86.8, 84.8, 81.7, 80.0, 73.9, 71.1, 68.9, 67.7, 60.3, 56.2, 55.3, 53.8, 52.5, 26.1. HRMS (ESI+): m/z calcd for $C_{26}H_{37}N_{12}O_9$ $[M+H]^+$: 661.2806, found: 661.2811.

4.1.11. Methyl (2S)-2-amino-4-({[(2R,5R)-5-(6-amino-9H-purin-9-yl)-3,4-dihydroxyoxolan-2-yl]methyl}(2-{[(2R,5R)-2-(6-amino-9H-purin-9-yl)-4-hydroxy-5-(hydroxymethyl)oxolan-3-yl]oxy}ethyl)amino)butanoate (3)

Following **method C** with **22** (140 mg, 0.12 mmol, 1.00 eq) and a 0–30% linear gradient of acetonitrile in TEAAc buffer 50 mM, pH 7 for purification, **3** (28 mg, 35%) was obtained as a white powder with 98% purity determined by HPLC analysis at 260 nm. ^{1}H NMR (600 MHz, D_2O) δ 8.08 (s, 1H), 8.05 (s, 1H), 7.98 (s, 1H), 7.84 (s, 1H), 5.89 (d, J = 2.5 Hz, 1H), 5.75 (d, J = 3.3 Hz, 1H), 4.55–4.50 (m, 1H), 4.47 (dd, J = 5.1 Hz, J = 2.3 Hz, 1H), 4.38 (dd, J = 5.0 Hz, J = 3.2 Hz, 1H), 4.36–4.30 (m, 1H), 4.26 (dd, J = 10.5 Hz, J = 2.8 Hz, 1H), 4.13 (dd, J = 7.9 Hz, J = 5.1 Hz, 1H), 4.07 (dt, J = 6.2 Hz, J = 3.1 Hz, 1H), 4.05–3.86 (m, 2H), 3.84 (s, 3H), 3.82–3.64 (m, 2H), 3.22–3.01 (m, 3H), 2.88 (dt, J = 13.7, J = 3.9, 1H), 2.78 (d, J = 13.9 Hz, 1H), 2.66–2.58 (m, 1H), 2.19–2.02 (m, 2H). ^{13}C NMR (150 MHz, D_2O) δ 170.6, 154.9 (2C), 152.5, 152.2, 147.7, 147.4, 139.1, 138.3, 118.5, 118.1, 89.1, 86.8, 84.6, 81.8, 79.6, 73.9, 70.9, 69.1, 60.2, 54.8, 54.1, 53.5, 53.3, 52.3, 25.0. HRMS (ESI+): m/z calcd for $C_{27}H_{39}N_{12}O_9$ $[M+H]^+$: 675.2957, found: 675.2944.

4.1.12. (2S)-2-amino-4-({[(2R,5R)-5-(6-amino-9H-purin-9-yl)-3,4-dihydroxyoxolan-2-yl]methyl}(2-{[(2R,5R)-2-(6-amino-9H-purin-9-yl)-4-hydroxy-5-(hydroxymethyl)oxolan-3-yl]oxy}ethyl)amino)butanamide (4)

Compound **22** (116 mg, 0.10 mmol, 1.00 eq) was treated at room temperature with TFA (1.44 mL) in water (360 μL) and stirred for 3 h at room temperature. The solvents were removed and the residue was treated with 7 M NH_3 in MeOH (10 mL). After stirring for 24 h at 30 °C, solvents were removed and the residue was purified by flash column chromatography on a reversed-phase silica gel column C_{18} (4 g, 40 μm) with a 0–15% linear gradient of acetonitrile in TEAAc buffer 50 mM, pH 7. The fractions containing the pure compound were pooled, concentrated and lyophilized with water to give **4** (23 mg, 38%) as a white powder with 98% purity determined by HPLC analysis at 260 nm. ^{1}H NMR (600 MHz, D_2O) δ 8.12 (s, 1H), 8.08 (s, 1H), 7.99 (s, 1H), 7.90 (s, 1H), 5.90 (d,

J = 2.7 Hz, 1H), 5.79 (d, J = 3.5 Hz, 1H), 4.53 (dd, J = 5.2 Hz, J = 2.7 Hz, 1H), 4.52–4.48 (m, 1H), 4.38 (dd, J = 5.0 Hz, J = 3.6 Hz, 1H), 4.35–4.28 (m, 1H), 4.18–4.07 (m, 3H), 3.98 (td, J = 10.7 Hz, J = 2.6 Hz, 1H), 3.88–3.80 (m, 2H), 3.72 (dd, J = 12.9 Hz, J = 3.5 Hz, 1H), 3.16–2.98 (m, 3H), 2.88–2.76 (m, 2H), 2.62 (dt, J = 14.0 Hz, J = 2.7 Hz, 1H), 2.17–1.98 (m, 2H). ^{13}C NMR (150 MHz, D_2O) δ 173.0, 155.0 (2C) 152.5, 152.3, 147.8, 147.6, 139.4, 138.7, 118.6, 118.3, 88.9, 86.8, 84.9, 81.8, 79.8, 73.8, 71.1, 69.0, 67.6, 60.4, 55.3, 53.9, 52.6, 52.4, 27.0. HRMS (ESI+): m/z calcd for $C_{26}H_{38}N_{13}O_8$ $[M+H]^+$: 660.2961, found: 660.2966.

4.1.13. General method D for the synthesis of compounds 23, 24 and 25

To a solution of **20** in anhydrous NMP (conc. 0.03 M) was added the corresponding bromide reagent (3.00 eq) and DIEA (3.00 eq). After stirring for 4 h at 110 °C under microwaves, the reaction mixture was diluted with AcOEt and brine. The aqueous layer was extracted with AcOEt and the combined organic extracts were washed with brine, dried over Na_2SO_4 and concentrated under vacuum. The residue was purified by flash column chromatography (silica gel, linear gradient 0–4% MeOH in DCM) to give the desired compound as a colorless solid.

4.1.14. 9-[(2R,5R)-3-[2-({[(4R,6R)-6-(6-amino-9H-purin-9-yl)-2,2-dimethyl-tetrahydro-2H-furo[3,4-d] [1,3]dioxol-4-yl]methyl}(butyl) amino)ethoxy]-4-[(tert-butyldimethylsilyl)oxy]-5-{[(tert-butyldimethylsilyl)oxy]methyl}oxolan-2-yl]-9H-purin-6-amine (23)

Following **method D** with **20** (80 mg, 97 μmol, 1.00 eq) and 1-bromobutane, **23** (40 mg, 47%) was obtained as a white solid. R_f 0.48 (MeOH/DCM 5:95). ^{1}H NMR (600 MHz, $CDCl_3$) δ 8.33 (s, 2H), 8.16 (s, 1H), 7.92 (s, 1H), 6.11 (d, J = 3.8 Hz, 1H), 6.03 (d, J = 2.3 Hz, 1H), 5.77 (br. s, 4H), 5.47 (dd, J = 6.4 Hz, J = 2.2 Hz, 1H), 4.91 (dd, J = 6.4 Hz, J = 3.2 Hz, 1H), 4.51 (t, J = 5.1 Hz, 1H), 4.37–4.24 (m, 2H), 4.09 (dt, J = 5.9 Hz, J = 3.0 Hz, 1H), 3.99 (dd, J = 11.5 Hz, J = 3.7 Hz, 1H), 3.76 (dd, J = 11.5 Hz, J = 2.8 Hz, 1H), 3.70–3.61 (m, 2H), 2.77–2.68 (m, 3H), 2.63 (dd, J = 13.5 Hz, J = 7.0 Hz, 1H), 2.46–2.37 (m, 2H), 1.59 (s, 3H), 1.38 (s, 3H), 1.31–1.22 (m, 2H), 1.22–1.12 (m, 2H), 0.92 (s, 9H), 0.91 (s, 9H), 0.82 (t, J = 7.3 Hz, 3H), 0.10–0.08 (m, 12H). ^{13}C NMR (150 MHz, $CDCl_3$) δ 155.6, 155.5, 153.2, 153.1, 149.8, 149.4, 140.2, 139.7, 120.5, 120.3, 114.4, 91.2, 87.2, 85.8, 84.9, 84.0, 83.4, 82.4, 69.9, 69.3, 62.0, 56.7, 55.1, 53.9, 29.2, 27.2, 26.1, 25.9, 25.5, 20.5, 18.6, 18.2, 14.1, −4.4, −4.6, −5.2, −5.2. HRMS (ESI+): m/z calcd for $C_{46}H_{72}N_{11}O_7Si_2$ $[M+H]^+$: 884.4998, found: 884.5002.

4.1.15. 9-[(2R,5R)-3-[2-({[(4R,6R)-6-(6-amino-9H-purin-9-yl)-2,2-dimethyl-tetrahydro-2H-furo[3,4-d] [1,3]dioxol-4-yl]methyl}(3-phenylpropyl)amino)ethoxy]-4-[(tert-butyldimethylsilyl)oxy]-5-{[(tert-butyldimethylsilyl)oxy]methyl}oxolan-2-yl]-9H-purin-6-amine (24)

Following **method D** with **20** (120 mg, 0.15 mmol, 1.00 eq) and 1-bromo-3-phenylpropane, **24** (75 mg, 53%) was obtained as a white solid. R_f 0.53 (MeOH/DCM 5:95).^{1}H NMR (600 MHz, $CDCl_3$) δ 8.31 (s, 1H), 8.28 (s, 1H), 8.15 (s, 1H), 7.90 (s, 1H), 7.25–7.08 (m, 5H), 6.11 (d, J = 3.7 Hz, 1H), 6.02 (d, J = 2.4 Hz, 1H), 5.81 (br. s, 4H), 5.46 (dd, J = 6.5 Hz, J = 2.1 Hz, 1H), 4.92 (dd, J = 6.5 Hz, J = 3.2 Hz, 1H), 4.50 (t, J = 5.1 Hz, 1H), 4.33–4.24 (m, 2H), 4.08 (dt, J = 5.9 Hz, J = 3.2 Hz, 1H), 3.98 (dd, J = 11.4 Hz, J = 3.6 Hz, 1H), 3.76 (dd, J = 11.5 Hz, J = 2.8 Hz, 1H), 3.72–3.60 (m, 2H), 2.80–2.70 (m, 3H), 2.64 (dd, J = 13.7 Hz, J = 6.7 Hz, 1H), 2.56–2.43 (m, 4H), 1.69–1.62 (m, 2H), 1.58 (s, 3H), 1.37 (s, 3H), 0.92 (s, 9H), 0.90 (s, 9H), 0.13–0.04 (m, 12H).^{13}C NMR (150 MHz, $CDCl_3$) δ 155.6, 155.5, 153.2, 153.1, 149.7, 149.4, 142.2, 140.2, 139.6, 128.4, 128.4, 125.8, 120.5, 120.3, 114.4, 91.1, 87.2, 85.7, 84.8, 83.9, 83.3, 82.5, 69.8, 69.3, 61.8, 56.7, 54.9, 53.9, 33.5, 28.8, 27.2, 26.1, 25.8, 25.5, 18.6, 18.2, −4.4, −4.6, −5.2, −5.2. HRMS (ESI+): m/z calcd for $C_{46}H_{72}N_{11}O_7Si_2$ $[M+H]^+$: 946.5155, found: 946.5149.

4.1.16. Methyl 4-({[(4R,6R)-6-(6-amino-9H-purin-9-yl)-2,2-dimethyl-tetrahydro-2H-furo[3,4-d] [1,3]dioxol-4-yl]methyl}(2-{[(2R,5R)-2-(6-amino-9H-purin-9-yl)-4-[(tert-butyldimethylsilyl) oxy]-5-{[(tert-butyldimethylsilyl)oxy]methyl}oxolan-3-yl]oxy} ethyl)amino)butanoate (25)

Following **method D** with **20** (600 mg, 0.73 mmol, 1.00 eq) and methyl-4-bromobutyrate, **25** (390 mg, 58%) was obtained as a white solid. R_f 0.34 (MeOH/DCM 5:95). ^{1}H NMR (600 MHz, $CDCl_3$) δ 8.32 (s, 1H), 8.31 (s, 1H), 8.17 (s, 1H), 7.90 (s, 1H), 6.11 (d, J = 3.6 Hz, 1H), 6.02 (m, 5H), 5.45 (dd, J = 6.5 Hz, J = 2.2 Hz, 1H), 4.91 (dd, J = 6.6 Hz, J = 3.3 Hz, 1H), 4.51 (t, J = 5.3 Hz, 1H), 4.32–4.23 (m, 2H), 4.08 (dt, J = 6.1 Hz, J = 3.2 Hz, 1H), 3.99 (dd, J = 11.5 Hz, J = 3.6 Hz, 1H), 3.76 (dd, J = 11.5 Hz, J = 2.8 Hz, 1H), 3.71–3.60 (m, 5H), 2.77 (dd, J = 13.5 Hz, J = 6.9 Hz, 1H), 2.74–2.69 (m, 2H), 2.64 (dd, J = 13.5 Hz, J = 6.8 Hz, 1H), 2.51–2.44 (m, 2H), 2.32–2.18 (m, 2H), 1.69–1.61 (m, 2H), 1.58 (s, 3H), 1.37 (s, 3H), 0.92 (s, 9H), 0.90 (s, 9H), 0.13–0.04 (m, 12H). ^{13}C NMR (150 MHz, $CDCl_3$) δ 174.0, 155.7, 155.6, 153.2, 153.1, 149.7, 149.4, 140.1, 139.5, 120.5, 120.3, 114.4, 91.1, 87.2, 85.7, 84.8, 83.9, 83.3, 82.5, 69.8, 69.3, 61.9, 56.7, 54.3, 53.7, 51.6, 31.5, 27.2, 26.1, 25.8, 25.5, 22.6, 18.6, 18.2, −4.4, −4.6, −5.2, −5.2. HRMS (ESI+): m/z calcd for $C_{42}H_{70}N_{11}O_9Si_2$ $[M+H]^+$: 928.4897, found: 928.4900.

4.1.17. (2R,5R)-2-(6-amino-9H-purin-9-yl)-5-{[(2-{[(2R,5R)-2-(6-amino-9H-purin-9-yl)-4-hydroxy-5-(hydroxymethyl)oxolan-3-yl] oxy}ethyl)(butyl)amino]methyl}oxolane-3,4-diol (5)

Following **method C** with **23** (40 mg, 0.45 mol, 1.00 eq) and a 0–50% linear gradient of acetonitrile in TEAAc buffer 50 mM, pH 7 for purification, **5** (20 mg, 72%) was obtained as a white powder with 98% purity determined by HPLC analysis at 260 nm.^{1}H NMR (500 MHz, DMSO-d_6) δ 8.36 (s, 1H), 8.32 (s, 1H), 8.14 (s, 1H), 8.13 (s, 1H), 7.33 (br. s, 2H), 7.25 (br. s, 2H), 5.97 (d, J = 6.3 Hz, 1H), 5.85 (d, J = 5.2 Hz, 1H), 5.49–5.39 (m, 3H), 5.14 (d, J = 5.3 Hz, 1H), 4.62 (q, J = 5.4 Hz, 1H), 4.52 (dd, J = 6.5, 4.7 Hz, 1H), 4.29 (dd, J = 4.8, 2.8 Hz, 1H), 4.06 (q, J = 4.9 Hz, 1H), 4.00–3.92 (m, 2H), 3.68–3.46 (m, 4H), 2.79 (dd, J = 14.0, 4.6 Hz, 1H), 2.70–2.51 (m, 3H), 2.41–2.30 (m, 2H), 1.22 (q, J = 7.4, 2H), 1.07 (tdd, J = 13.4 Hz, J = 10.5 Hz, J = 6.3 Hz, 2H), 0.73 (t, J = 7.3 Hz, 2H). ^{13}C NMR (125 MHz, DMSO-d_6) δ 156.2, 156.0, 152.6, 152.4, 149.3, 148.9, 139.8, 139.8, 119.3, 119.1, 87.5, 86.3, 86.2, 82.4, 81.2, 72.5, 71.9, 69.2, 67.9, 61.5, 56.1, 54.0, 53.7, 28.3, 19.8, 13.7. HRMS (ESI+): m/z calcd for $C_{26}H_{38}N_{11}O_7$ $[M+H]^+$: 616.2956, Found 616.2955.

4.1.18. (2R,5R)-2-(6-amino-9H-purin-9-yl)-5-{[(2-{[(2R,5R)-2-(6-amino-9H-purin-9-yl)-4-hydroxy-5-(hydroxymethyl)oxolan-3-yl] oxy}ethyl)(3-phenylpropyl)amino]methyl}oxolane-3,4-diol (6)

Following **method C** with **24** (40 mg, 0.42 μmol, 1.00 eq) and a 0–50% linear gradient of acetonitrile in TEAAc buffer 50 mM, pH 7 for purification, **6** (8 mg, 28%) was obtained as a white powder with 99% purity determined by HPLC analysis at 260 nm. ^{1}H NMR (500 MHz, DMSO-d_6) δ 8.36 (s, 1H), 8.32 (s, 1H), 8.14 (s, 1H), 8.13 (s, 1H), 7.33 (br. s, 2H), 7.25 (br. s, 2H), 5.97 (d, J = 6.3 Hz, 1H), 5.85 (d, J = 5.2 Hz, 1H), 5.49–5.39 (m, 3H), 5.14 (d, J = 5.3 Hz, 1H), 4.62 (q, J = 5.4 Hz, 1H), 4.52 (dd, J = 6.5, 4.7 Hz, 1H), 4.29 (dd, J = 4.8, 2.8 Hz, 1H), 4.06 (q, J = 4.9 Hz, 1H), 4.00–3.92 (m, 2H), 3.68–3.46 (m, 4H), 2.79 (dd, J = 14.0, 4.6 Hz, 1H), 2.70–2.51 (m, 3H), 2.41–2.30 (m, 2H), 1.22 (q, J = 7.4, 2H), 1.07 (tdd, J = 13.4 Hz, J = 10.5 Hz, J = 6.3 Hz, 2H), 0.73 (t, J = 7.3 Hz, 2H). ^{13}C NMR (125 MHz, DMSO-d_6) δ 156.1, 156.0, 152.5, 152.4, 149.3, 149.0, 139.8, 139.8, 119.3, 119.2, 87.6, 86.3, 86.2, 82.4, 81.2, 72.5, 71.9, 69.2, 68.0, 62.0, 56.2, 54.0, 53.7, 28.3, 19.8, 13.8. HRMS (ESI+): m/z calcd for $C_{26}H_{38}N_{11}O_7$ $[M+H]^+$: 616.2956, Found 616.2955.

4.1.19. Methyl 4-({[(2R,5R)-5-(6-amino-9H-purin-9-yl)-3,4-dihydroxyoxolan-2-yl]methyl}(2-{[(2R,5R)-2-(6-amino-9H-purin-9-yl)-4-hydroxy-5-(hydroxymethyl)oxolan-3-yl]oxy}ethyl)amino) butanoate (7)

Following **method C** with **25** (116 mg, 0.13 mmol, 1.00 eq) and a 0–50% linear gradient of acetonitrile in TEAAc buffer 50 mM, pH 7 for purification, **7** (51 mg, 60%) was obtained as a white powder with 97% purity determined by HPLC analysis at 260 nm. ^{1}H NMR (500 MHz, DMSO-d_6) δ 8.37 (s, 1H), 8.33 (s, 1H), 8.14 (s, 1H), 8.13 (s, 1H), 7.38 (br. s, 2H), 7.29 (br. s, 2H), 5.97 (d, J = 6.3 Hz, 1H), 5.84 (d, J = 5.3 Hz, 1H), 5.52–5.32 (m, 3H), 5.19 (d, J = 5.3 Hz, 1H), 4.62 (q, J = 5.4 Hz, 1H), 4.49 (dd, J = 6.3, 4.7 Hz, 1H), 4.30 (dd, J = 4.8, 2.8 Hz, 1H), 4.04 (q, J = 4.9 Hz, 1H), 3.99–3.96 (m, 1H), 3.95–3.87 (m, 1H), 3.66 (dt, J = 12.1, 4.1 Hz, 1H), 3.62–3.45 (m, 6H), 2.79 (dd, J = 14.1, 4.6 Hz, 1H), 2.71–2.52 (m, 3H), 2.45–2.28 (m, 2H), 2.14 (td, J = 7.4, 5.9 Hz, 2H), 1.58–1.46 (m, 2H). ^{13}C NMR (125 MHz, DMSO-d_6) δ 173.3, 156.2, 156.1, 152.6, 152.5, 149.4, 148.9, 139.9, 139.8, 119.4, 119.2, 87.6, 86.4, 86.3, 82.4, 81.3, 72.6, 71.9, 69.2, 68.0, 61.6, 56.3, 53.5, 53.4, 51.2, 30.9, 21.8. HRMS (ESI+): m/z calcd for $C_{27}H_{38}N_{11}O_9$ $[M+H]^+$: 660.2854, Found 660.2855.

4.1.20. 4-({[(2R,5R)-5-(6-amino-9H-purin-9-yl)-3,4-dihydroxyoxolan-2-yl]methyl}(2-[(2R,5R)-2-(6-amino-9H-purin-9-yl)-4-hydroxy-5-(hydroxymethyl)oxolan-3-yl]oxy}ethyl)amino) butanoic acid (8)

Compound **25** (140 mg, 0.15 mmol, 1.00 eq) was treated with TFA (1.37 mL) and water (0.34 mL). After stirring for 5.5 h, solvents were removed under vacuum. The residue was dissolved in water (0.5 mL) and 2 M LiOH aqueous solution (3.5 mL) was added. After stirring at 0 °C for 30 min, pH was adjusted to ≈3 or 4 by addition of 1 M HCl aqueous solution. Solvents were removed under vacuum and the residue was purified by flash column chromatography on a reversed-phase silica gel column C_{18} (4 g, 40 μm) with a 0–20% linear gradient of acetonitrile in TEAAc buffer 50 mM, pH 7. The fractions containing the pure compound were pooled, concentrated and lyophilized with water and 1,4-dioxane to give **8** (35 mg, 36%) as a white powder with 99% purity determined by HPLC analysis at 260 nm. ^{1}H NMR (600 MHz, D_2O) δ 8.24 (s, 1H), 8.13 (s, 1H), 8.05 (s, 1H), 8.01 (s, 1H), 5.98 (d, J = 4.3 Hz, 1H), 5.94 (d, J = 4.6 Hz, 1H), 4.68–4.59 (m, 1H), 4.51–4.44 (m, 2H), 4.44–4.38 (m, 1H), 4.38–4.30 (m, 1H), 4.23–4.15 (m, 1H), 4.09–3.95 (m, 2H), 3.91 (dd, J = 12.9, J = 2.7 Hz, 1H), 3.80 (dd, J = 12.9, J = 3.8 Hz, 1H), 3.69–3.33 (m, 4H), 3.20 (m, 2H), 2.29 (td, J = 7.0 Hz, J = 2.7 Hz, 2H), 2.02–1.85 (m, 2H). ^{13}C NMR (150 MHz, D_2O) δ 174.5, 154.9 (2C), 152.5, 152.3, 147.7, 147.5, 139.3, 138.5, 118.6, 118.3, 89.0, 86.9, 84.8, 81.8, 80.1, 73.9, 71.1, 69.0, 67.8, 60.3, 56.2, 55.3, 53.8, 52.5, 26.1. HRMS (ESI+): m/z calcd for $C_{26}H_{37}N_{12}O_9$ $[M+H]^+$: 661.2806, found: 661.2811.

4.1.21. N-{[(2R,5R)-5-(6-amino-9H-purin-9-yl)-3,4-dihydroxyoxolan-2-yl]methyl}-N-(2-{[(2R,5R)-2-(6-amino-9H-purin-9-yl)-4-hydroxy-5-(hydroxymethyl)oxolan-3-yl]oxy}ethyl)-4-nitrobenzene-1-sulfonamide (9)

Using **method C** with **19** (100 mg, 97.4 μmol, 1.00 eq) and a 0–40% linear gradient of acetonitrile in TEAAc buffer 50 mM, pH 7 for purification, **9** (25 mg, 34%) was obtained as a white powder with 99% purity determined by HPLC analysis at 260 nm. ^{1}H NMR (600 MHz, DMSO-d_6) δ 8.32 (s, 1H), 8.29 (s, 1H), 8.22–8.18 (m, 2H), 8.14 (s, 1H), 8.13 (s, 1H), 7.96–7.91 (m, 2H), 7.32 (br. s, 2H), 7.26 (br. s, 2H), 5.89 (d, J = 5.4 Hz, 1H), 5.79 (d, J = 5.6 Hz, 1H), 5.73–5.20 (m, 4H), 4.70 (t, J = 5.4 Hz, 1H), 4.34 (t, J = 5.1 Hz, 1H), 4.30–4.26 (m, 1H), 4.15 (t, J = 4.6 Hz, 1H), 4.09 (dt, J = 8.5 Hz, J = 4.3 Hz, 1H), 3.89 (q, J = 3.6 Hz, 1H), 3.75–3.70 (m, 2H), 3.66–3.63 (m, 1H), 3.60–3.29 (m, 5H). ^{13}C NMR (150 MHz, DMSO-d_6) δ 156.2, 156.2, 152.8, 152.7, 149.6, 149.3, 149.0, 145.0, 140.2, 139.6, 128.5, 124.3, 119.3, 119.3, 87.9, 86.3, 86.0, 82.9, 81.6, 72.5, 71.4, 70.0, 68.2, 61.2, 50.4, 47.5. HRMS (ESI+): m/z calcd for $C_{28}H_{33}N_{12}O_{11}S$ $[M+H]^+$: 745.2112, Found 745.2104.

4.1.22. N-{[(4R,6R)-6-(6-amino-9H-purin-9-yl)-2,2-dimethyl-tetrahydro-2H-furo[3,4-d] [1,3]dioxol-4-yl]methyl}-4-methoxy-2-nitrobenzene-1-sulfonamide (26)

Following **method A** with 5′-amino-2′,3′-isopropylidene adenosine (280 mg, 0.92 mmol, 1.00 eq) and 4-methoxy-2-nitrobenzenesufonyl chloride, **26** (191 mg, 40%) was obtained as a beige solid. R_f 0.59 (8:92 MeOH/DCM). ^{1}H NMR (600 MHz, DMSO-d_6) δ 8.43 (t, J = 5.8 Hz, 1H), 8.28 (s, 1H), 8.12 (s, 1H), 7.74 (d, J = 8.9 Hz, 1H), 7.51 (d, J = 2.6 Hz, 1H), 7.40 (br. s, 2H), 7.20 (dd, J = 8.9 Hz, J = 2.6 Hz, 1H), 6.11 (d, J = 3.0 Hz, 1H), 5.36 (dd, J = 6.3 Hz, J = 3.0 Hz, 1H), 4.93 (dd, J = 6.4 Hz, J = 2.9 Hz, 1H), 4.23 (td, J = 5.8 Hz, J = 2.9 Hz, 1H), 3.87 (s, 3H), 3.27–3.14 (m, 2H), 1.52 (s, 3H), 1.28 (s, 3H). ^{13}C NMR (150 MHz, DMSO-d_6) δ 162.5, 156.2, 153.0, 149.0, 148.3, 140.2, 131.3, 123.8, 119.3, 117.2, 113.5, 109.8, 89.5, 84.1, 82.8, 81.5, 56.6, 44.5, 27.0, 25.1. HRMS (ESI+): m/z calcd for $C_{20}H_{24}N_7O_8S$ $[M+H]^+$: 522.1407, Found 522.1407.

4.1.23. N-{[(4R,6R)-6-(6-amino-9H-purin-9-yl)-2,2-dimethyl-tetrahydro-2H-furo[3,4-d] [1,3]dioxol-4-yl]methyl}-2-methoxy-4-nitrobenzene-1-sulfonamide (27)

Following **method A** with 5′-amino-2′,3′-isopropylidene adenosine (280 mg, 0.92 mmol, 1.00 eq) and 2-methoxy-4-nitrobenzenesufonyl chloride, **27** (200 mg, 42%) was obtained as a beige solid. R_f 0.59 (8:92 MeOH/DCM). ^{1}H NMR (600 MHz, DMSO-d_6) δ 8.30 (t, J = 5.4 Hz, 1H), 8.23 (s, 1H), 8.12 (s, 1H), 7.88–7.82 (m, 2H), 7.77 (dd, J = 8.5 Hz, J = 2.2 Hz, 1H), 7.37 (br. s, 2H), 6.06 (d, J = 2.9 Hz, 1H), 5.31 (dd, J = 6.3 Hz, J = 3.0 Hz, 1H), 4.90 (dd, J = 6.4 Hz, J = 2.9 Hz, 1H), 4.16 (td, J = 5.7 Hz, J = 2.9 Hz, 1H), 3.88 (s, 3H), 3.24–3.12 (m, 2H), 1.49 (s, 3H), 1.27 (s, 3H). ^{13}C NMR (150 MHz, DMSO-d_6) δ 156.7, 156.2, 152.6, 150.8, 148.3, 140.1, 133.5, 130.3, 119.3, 114.8, 113.4, 107.7, 89.5, 84.2, 82.9, 81.5, 56.8, 44.7, 26.9, 25.1. HRMS (ESI+): m/z calcd for $C_{20}H_{24}N_7O_8S$ $[M+H]^+$: 522.1407, Found 522.1407.

4.1.24. N-{[(4R,6R)-6-(6-amino-9H-purin-9-yl)-2,2-dimethyl-tetrahydro-2H-furo[3,4-d] [1,3]dioxol-4-yl]methyl}-2-nitro-4-(trifluoromethyl)benzene-1-sulfonamide (28)

To a solution of 5′-amino-2′,3′-isopropylidene adenosine (280 mg, 0.92 mmol, 1.00 eq) in anhydrous DMF (4.6 mL) was added Et_3N (250 μL, 1.83 mmol, 2.00 eq). 2-nitro-4-trifluoromethylbenzenesufonyl chloride (396 mg, 1.37 mmol, 1.50 eq) was added at 0 °C and the reaction mixture was stirred for 4 h at room temperature under argon. The reaction mixture was diluted with AcOEt (30 mL) and water (30 mL). The aqueous layer was extracted with AcOEt (3 × 30 mL) and the combined organic extracts were washed with brine (30 mL), dried over Na_2SO_4 and concentrated under vacuum. The residue was purified by flash column chromatography (silica gel, linear gradient 0–5% MeOH in DCM) to give **28** (230 mg, 45%) as a dark red solid. R_f 0.34 (8:92 MeOH/CH_2Cl_2). ^{1}H NMR (500 MHz, DMSO-d_6) δ 8.93 (t, J = 5.1 Hz, 1H), 8.50 (d, J = 1.8 Hz, 1H), 8.28 (s, 1H), 8.14 (s, 1H), 8.10 (dd, J = 1.6 Hz, J = 8.6 Hz, 1H), 8.04 (d, J = 8.3 Hz), 7.45 (br. s, 2H), 6.11 (d, J = 2.9 Hz, 1H), 5.34 (dd, J = 6.3 Hz, J = 2.9 Hz, 1H), 4.92 (dd, J = 6.3 Hz, J = 3.1 Hz, 1H), 4.20 (td, J = 5.9 Hz, J = 3.1 Hz, 1H), 3.37–3.25 (m, 2H), 1.50 (s, 3H), 1.27 (s, 3H). ^{13}C NMR (125 MHz, DMSO-d_6) δ 156.1, 152.4, 148.4, 147.6, 140.2, 136.4, 133.8, 133.5, 133.2, 133.0, 130.8, 129.4, 125.5, 123.4, 121.2, 119.0, 122.0, 122.0, 119.3, 113.5, 107.7, 89.4, 84.3, 83.0, 81.5, 44.7, 26.9, 25.0. HRMS (ESI+): m/z calcd for $C_{20}H_{21}N_7O_7SF_3$ $[M+H]^+$: 560.1175, Found 560.1180.

4.1.25. N-{[(4R,6R)-6-(6-amino-9H-purin-9-yl)-2,2-dimethyl-tetrahydro-2H-furo[3,4-d] [1,3]dioxol-4-yl]methyl}-4-chloro-3-nitrobenzene-1-sulfonamide (29)

Following **method A** with 5′-amino-2′,3′-isopropylidene adenosine (280 mg, 0.92 mmol, 1.00 eq) and 4-chloro-3-nitrobenzenesufonyl chloride, **29** (346 mg, 72%) was obtained as a brown solid. R_f 0.42 (8:92 MeOH/CH_2Cl_2). ^{1}H NMR (400 MHz, DMSO-d_6) δ 8.56 (s, 1H), 8.39 (d, J = 2.1 Hz, 1H), 8.27 (s, 1H), 8.14 (s, 1H), 7.96 (dd, J = 8.5 Hz, J = 2.1 Hz, 1H), 7.90 (d, J = 8.5 Hz, 1H), 7.37 (br. s, 2H), 6.12 (d, J = 2.8 Hz, 1H), 5.34 (dd, J = 6.3 Hz, J = 2.9 Hz, 1H), 4.89 (dd, J = 6.3 Hz, J = 3.1 Hz, 1H) 4.17 (td, J = 5.9 Hz, J = 3.0 Hz, 1H), 3.33−3.18 (m, 2H), 1.51 (s, 3H), 1.29 (s, 3H). ^{13}C NMR (100 MHz, DMSO-d_6) δ 156.7, 153.0, 148.9, 147.8, 141.1, 140.6, 133.4, 131.6, 129.8, 124.4, 119.7, 114.0, 107.7, 89.8, 84.7, 83.4, 82.0, 44.9, 27.4, 25.6. HRMS (ESI+): m/z calcd for $C_{19}H_{21}N_7O_7SCl$ $[M+H]^+$: 526.0912, Found 526.0914.

4.1.26. N-{[(4R,6R)-6-(6-amino-9H-purin-9-yl)-2,2-dimethyl-tetrahydro-2H-furo[3,4-d] [1,3]dioxol-4-yl]methyl}-N-(2-{[(2R,5R)-2-(6-amino-9H-purin-9-yl)-4-[(tert-butyldimethylsilyl)oxy]-5-{[(tert-butyldimethylsilyl)oxy]methyl}oxolan-3-yl]oxy}ethyl)-4-methoxy-2-nitrobenzene-1-sulfonamide (30)

Following **method B** with **26** (161 mg, 0.31 mmol, 1.00 eq), **30** (166 mg, 52%) was obtained as a pale white solid. R_f 0.67 (10:90 MeOH/DCM). ^{1}H NMR (500 MHz, $CDCl_3$)) δ 8.286 (s, 1H), 8.292 (s, 1H), 8.14 (s, 1H), 7.82 (s, 1H), 7.66 (d, J = 8.9 Hz, 1H), 6.92 (d, J = 2.6 Hz, 1H), 6.74 (dd, J = 9.0 Hz, J = 2.6 Hz, 1H), 6.01 (d, J = 3.2 Hz, 1H), 5.97−5.88 (m, 5H), 5.31 (dd, J = 6.5 Hz, J = 2.1 Hz, 1H), 4.99 (dd, J = 6.4 Hz, J = 3.7 Hz, 1H), 4.52 (dd, J = 6.1 Hz, J = 4.6 Hz, 1H), 4.43 (dt, J = 8.4 Hz, J = 4.2 Hz, 1H), 4.22 (dd, J = 4.7 Hz, J = 3.2 Hz, 1H), 4.06 (dt, J = 6.1 Hz, J = 3.1 Hz, 1H), 3.97 (dd, J = 11.5 Hz, J = 3.5 Hz, 1H), 3.86−3.49 (m, 10H), 1.55 (s, 3H), 1.33 (s, 3H), 0.90 (br. s, 18H), 0.11−0.05 (m, 12H). ^{13}C NMR (125 MHz, $CDCl_3$) δ 162.8, 155.7, 155.5, 153.2, 152.9, 149.6, 149.1, 149.0, 140.2, 139.7, 133.0, 125.0, 120.4, 120.3, 116.2, 114.7, 109.9, 90.6, 87.4, 84.5, 84.5 (2C), 84.3, 82.6, 82.5, 69.9, 69.6, 61.6, 50.2, 47.2, 27.3, 26.2, 25.9, 25.4, 18.6, 18.2, −4.4, −4.7, −5.3. HRMS (ESI+): m/z calcd for $C_{47}H_{67}N_{12}O_{12}SSi_2$ $[M+H]^+$: 1043.4261, found: 1043.4265.

4.1.27. N-{[(4R,6R)-6-(6-amino-9H-purin-9-yl)-2,2-dimethyl-tetrahydro-2H-furo[3,4-d] [1,3]dioxol-4-yl]methyl}-N-(2-{[(2R,5R)-2-(6-amino-9H-purin-9-yl)-4-[(tert-butyldimethylsilyl)oxy]-5-{[(tert-butyldimethylsilyl)oxy]methyl}oxolan-3-yl]oxy}ethyl)-2-methoxy-4-nitrobenzene-1-sulfonamide (31)

Following **method B** with **27** (185 mg, 0.36 mmol, 1.00 eq), **31** (160 mg, 43%) was obtained as a pale white solid. R_f 0.67 (10:90 MeOH/DCM). ^{1}H NMR (500 MHz, $CDCl_3$) δ 8.30 (s, 1H), 8.29 (s, 1H), 8.16 (br. s, 1H), 7.82 (s, 1H), 7.67 (m, 2H), 7.57−7.43 (m, 2H), 6.16−5.90 (m, 5H), 5.88 (s, 1H), 5.27 (br. s, 1H), 4.94 (dd, J = 6.7 Hz, J = 3.7 Hz, 1H), 4.52 (t, J = 5.4 Hz, 1H), 4.42 (dt, J = 8.7 Hz, J = 4.2 Hz, 1H), 4.20 (dd, J = 4.7 Hz, J = 3.1 Hz, 1H), 4.07 (dt, J = 6.1 Hz, J = 3.0 Hz, 1H), 3.99 (dd, J = 11.5 Hz, J = 3.4 Hz, 1H), 3.92−3.44 (m, 10H), 1.54 (s, 3H), 1.32 (s, 3H), 0.921 (br. s, 9H), 0.918 (br. s, 9H), 0.15−0.05 (m, 12H). ^{13}C NMR (125 MHz, $CDCl_3$) δ 157.1, 155.8, 155.5, 153.2, 152.9, 150.9, 149.5, 148.9, 139.7, 139.6, 134.2, 131.5, 120.4, 120.2, 114.7 (2C), 106.7, 90.5, 87.5, 84.5, 84.4, 84.4, 82.8, 82.6, 70.7, 69.6, 61.5, 56.8, 50.2, 47.1, 27.2, 26.2, 25.9, 25.4, 18.6, 18.2, −4.3, −4.8, −5.2. HRMS (ESI+): m/z calcd for $C_{47}H_{67}N_{12}O_{12}SSi_2$ $[M+H]^+$: 1043.4261, found: 1043.4255.

4.1.28. N-{[(4R,6R)-6-(6-amino-9H-purin-9-yl)-2,2-dimethyl-tetrahydro-2H-furo[3,4-d] [1,3]dioxol-4-yl]methyl}-N-(2-{[(2R,5R)-2-(6-amino-9H-purin-9-yl)-4-[(tert-butyldimethylsilyl)oxy]-5-{[(tert-butyldimethylsilyl)oxy]methyl}oxolan-3-yl]oxy}ethyl)-2-nitro-4-(trifluoromethyl)benzene-1-sulfonamide (32)

Following **method B** with **28** (77 mg, 0.14 mmol, 1.00 eq), **32** (68 mg, 46%) was obtained as a pale white solid. R_f 0.47 (10:90 MeOH/DCM). ^{1}H NMR (500 MHz, $CDCl_3$) δ 8.33 (s, 1H), 8.30 (s, 1H), 8.15 (s, 1H), 7.85 (d, J = 8.2 Hz, 1H), 7.77 (d, J = 1.7 Hz, 1H), 7.76 (s, 1H), 7.54 (dd, J = 8.4 Hz, J = 1.8 Hz, 1H), 5.97 (d, J = 2.8 Hz, 1H), 5.93 (d, J = 1.9 Hz, 1H), 5.74 (br. s, 4H), 5.33 (dd, J = 6.4 Hz, J = 2.0 Hz, 1H), 5.01 (dd, J = 6.4 Hz, J = 3.8 Hz, 1H), 4.50 (dd, J = 6.4 Hz, J = 4.6 Hz, 1H), 4.43 (dt, J = 8.3 Hz, J = 4.0 Hz, 1H), 4.18 (dd, J = 4.7 Hz, J = 2.8 Hz, 1H), 4.01−3.96 (m, 2H), 3.94−3.78 (m, 4H), 3.77−3.66 (m, 2H), 3.56 (dt, J = 15.5 Hz, J = 5.1 Hz, 1H), 1.55 (s, 3H), 1.34 (s, 3H), 0.91 (s, 9H), 0.89 (s, 9H), 0.13−0.02 (m, 12H). ^{13}C NMR (125 MHz, $CDCl_3$) δ 155.6, 155.4, 153.3, 153.0, 149.5, 149.1, 147.9, 140.2, 139.5, 137.4, 135.6, 135.3, 135.0, 134.7, 132.0, 128.3, 128.3, 125.3, 123.2, 121.0, 118.8, 121.7, 121.6, 133.0, 120.4, 120.3, 116.2, 114.8, 109.9, 90.6, 87.5, 84.7, 84.3, 84.1, 82.9, 82.6, 69.6, 69.4, 61.3, 50.2, 47.4, 27.2, 26.2, 25.9, 25.4, 18.6, 18.2, −4.4, −4.8, −5.3. HRMS (ESI+): m/z calcd for $C_{44}H_{64}N_{12}O_{11}SF_3Si_2$ $[M+H]^+$: 1081.4029, found: 1081.4034.

4.1.29. N-{[(4R,6R)-6-(6-amino-9H-purin-9-yl)-2,2-dimethyl-tetrahydro-2H-furo[3,4-d] [1,3]dioxol-4-yl]methyl}-N-(2-{[(2R,5R)-2-(6-amino-9H-purin-9-yl)-4-[(tert-butyldimethylsilyl)oxy]-5-{[(tert-butyldimethylsilyl)oxy]methyl}oxolan-3-yl]oxy}ethyl)-4-chloro-3-nitrobenzene-1-sulfonamide (33)

Following **method B** with **29** (230 mg, 0.44 mmol, 1.00 eq), **33** (160 mg, 43%) was obtained as a pale white solid. R_f 0.52 (10:90 MeOH/DCM). ^{1}H NMR (600 MHz, $CDCl_3$) δ 8.29 (s, 1H), 8.28 (s, 1H), 8.116 (2s, 2H), 7.79 (s, 1H), 7.65 (dd, J = 8.4 Hz, J = 2.1 Hz, 1H), 7.39 (d, J = 8.4 Hz, 1H), 6.02−5.93 (m, 6H), 5.36 (dd, J = 6.4 Hz, J = 1.8 Hz, 1H), 5.05 (dd, J = 6.4 Hz, J = 3.8 Hz, 1H), 4.51 (dd, J = 6.1 Hz, J = 4.7 Hz, 1H), 4.44 (dt, J = 8.5 Hz, J = 4.3 Hz, 1H), 4.19 (dd, J = 4.7 Hz, J = 3.0 Hz, 1H), 4.05−3.97 (m, 2H), 3.82 (t, J = 5.5 Hz, 2H), 3.79−3.65 (m, 3H), 3.46 (q, J = 5.3 Hz, 2H), 1.56 (s, 3H), 1.35 (s, 3H), 0.92 (br. s, 9H), 0.90 (br. s, 9H), 0.12−0.05 (m, 12H). ^{13}C NMR (150 MHz, $CDCl_3$) δ 155.8, 155.6, 153.2, 153.1, 149.5, 149.0, 147.6, 140.3, 140.2, 139.4, 132.4, 131.3, 131.2, 124.6, 120.5, 120.2, 114.7, 90.7, 87.4, 85.0, 84.3 (2C), 82.9, 82.6, 69.7, 69.5, 61.4, 50.5, 47.7, 27.2, 26.2, 25.9, 25.4, 18.6, 18.2, −4.4, −4.7, −5.2. HRMS (ESI+): m/z calcd for $C_{43}H_{64}N_{12}O_{11}SSi_2Cl$ $[M+H]^+$: 1047.3765, found: 1047.3766.

4.1.30. N-(((2R,3S,4R,5R)-5-(6-amino-9H-purin-9-yl)-3,4-dihydroxytetrahydrofuran-2-yl)methyl)-N-(2-(((2R,3R,4R,5R)-2-(6-amino-9H-purin-9-yl)-4-hydroxy-5-(hydroxymethyl) tetrahydrofuran-3-yl)oxy)ethyl)-4-methoxy-2-nitrobenzenesulfonamide (10)

Using **method C** with **30** (167 mg, 0.16 mmol, 1.00 eq) and a 0−40% linear gradient of acetonitrile in TEAAc buffer 50 mM, pH 7 for purification, **10** (25 mg, 20%) was obtained as a white powder with 97% purity determined by HPLC analysis at 260 nm. ^{1}H NMR (500 MHz, DMSO-d_6) δ 8.32 (s, 1H), 8.28 (s, 1H), 8.13 (s, 2H), 7.77 (d, J = 9.0 Hz, 1H), 7.44 (dd, J = 8.5 Hz, J = 2.6 Hz, 1H), 7.34 (br. s, 2H), 7.29 (br. s, 2H), 6.99 (dd, J = 9.0 Hz, J = 2.6 Hz, 1H), 5.95 (d, J = 5.2 Hz, 1H), 5.83 (d, J = 5.5 Hz, 1H), 5.65 (br. s, 1H), 5.49 (br. s, 1H), 5.38 (t, J = 5.7 Hz, 1H), 5.27 (br. s, 1H), 4.66 (t, J = 5.2 Hz, 1H), 4.37 (t, J = 5.1 Hz, 1H), 4.33−4.26 (m, 1H), 4.17−4.08 (m, 2H), 3.93 (q, J = 3.6 Hz, 1H), 3.84 (s, 3H), 3.80−3.62 (m, 3H), 3.60−3.37 (m, 5H). ^{13}C NMR (125 MHz, DMSO-d_6) δ 162.6, 156.1, 156.2, 152.6, 152.6, 149.3, 149.0, 148.9, 139.9, 139.8, 131.5, 123.3, 119.2 (2C), 116.7, 109.7, 87.8, 86.3, 85.8, 81.8, 81.5, 72.5, 71.5, 68.1, 66.4, 61.1, 56.6, 50.3, 47.1. HRMS (ESI+): m/z calcd for $C_{29}H_{35}N_{12}O_{12}S$ $[M+H]^+$: 775.2218, Found 775.2225.

4.1.31. N-{[(2R,5R)-5-(6-amino-9H-purin-9-yl)-3,4-dihydroxyoxolan-2-yl]methyl}-N-(2-{[(2R,5R)-2-(6-amino-9H-purin-9-yl)-4-hydroxy-5-(hydroxymethyl)oxolan-3-yl]oxy}ethyl)-2-methoxy-4-nitrobenzene-1-sulfonamide (11)

Using **method C** with **31** (160 mg, 0.15 mmol, 1.00 eq) and a 0–40% linear gradient of acetonitrile in TEAAc buffer 50 mM, pH 7 for purification, **11** (15 mg, 13%) was obtained as a white powder with 98% purity determined by HPLC analysis at 260 nm. ^{1}H NMR (500 MHz, DMSO-d_6) δ 8.32 (s, 1H), 8.28 (s, 1H), 8.13 (s, 2H), 7.77 (d, J = 9.0 Hz, 1H), 7.44 (dd, J = 8.5 Hz, J = 2.6 Hz, 1H), 7.34 (br. s, 2H), 7.29 (br. s, 2H), 6.99 (dd, J = 9.0 Hz, J = 2.6 Hz, 1H), 5.95 (d, J = 5.2 Hz, 1H), 5.83 (d, J = 5.5 Hz, 1H), 5.65 (br. s, 1H), 5.49 (br. s, 1H), 5.38 (t, J = 5.7 Hz, 1H), 5.27 (br. s, 1H), 4.66 (t, J = 5.2 Hz, 1H), 4.37 (t, J = 5.1 Hz, 1H), 4.33–4.27 (m, 1H), 4.17–4.08 (m, 2H), 3.93 (q, J = 3.6 Hz, 1H), 3.84 (s, 3H), 3.80–3.62 (m, 3H), 3.60–3.37 (m, 5H). ^{13}C NMR (125 MHz, DMSO-d_6) δ 156.9, 156.1, 155.9, 152.5, 152.4, 150.6, 149.0, 148.8, 134.0, 139.5, 133.7, 131.0, 119.2, 119.2, 114.4, 107.4, 87.8, 86.2, 85.9, 81.5, 81.4, 72.5, 71.3, 68.9, 66.7, 61.1, 56.8, 50.2, 47.1. HRMS (ESI+): m/z calcd for $C_{29}H_{35}N_{12}O_{12}S$ $[M+H]^+$: 775.2218, Found 775.2220.

4.1.32. N-{[(2R,5R)-5-(6-amino-9H-purin-9-yl)-3,4-dihydroxyoxolan-2-yl]methyl}-N-(2-{[(2R,5R)-2-(6-amino-9H-purin-9-yl)-4-hydroxy-5-(hydroxymethyl)oxolan-3-yl]oxy}ethyl)-2-nitro-4-(trifluoromethyl)benzene-1-sulfonamide (12)

Using **method C** with (120 mg, 0.11 mmol, 1.00 eq) and a 0–40% linear gradient of acetonitrile in TEAAc buffer 50 mM, pH 7 for purification, **12** (18 mg, 20%) was obtained as a white powder with 99% purity determined by HPLC analysis at 260 nm. ^{1}H NMR (500 MHz, DMSO-d_6) δ 8.47 (d, J = 1.7 Hz, 1H), 8.32 (s, 1H), 8.28 (s, 1H), 8.15 (d, J = 8.3 Hz, 1H), 8.12 (s, 1H), 8.11 (s, 1H), 7.88 (dd, J = 8.6 Hz, J = 1.8 Hz, 1H), 7.36 (br. s, 2H), 7.31 (br. s, 2H), 5.90 (d, J = 5.2 Hz, 1H), 5.82 (d, J = 5.4 Hz, 1H), 5.61 (d, J = 6.0 Hz, 1H), 5.43 (d, J = 5.1 Hz, 1H), 5.38 (dd, J = 6.6 Hz, J = 4.8 Hz, 1H), 5.30 (d, J = 5.3 Hz, 1H), 4.65 (q, J = 5.4 Hz, 1H), 4.37 (t, J = 5.1 Hz, 1H), 4.31 (q, J = 4.7 Hz, 1H), 4.19–4.10 (m, 2H), 3.91 (q, J = 3.6 Hz, 1H), 3.87–3.63 (m, 4H), 3.61–3.45 (m, 4H). ^{13}C NMR (125 MHz, DMSO-d_6) δ 156.2, 156.1, 152.7, 152.6, 149.2, 148.9, 147.7, 139.9, 139.4, 135.9, 133.9, 133.6, 133.3, 133.1, 131.1, 128.9, 128.9, 152.5, 123.3, 121.1, 119.0, 122.0, 121.9, 119.2 (2C), 87.8, 86.3, 85.9, 81.6, 81.5, 72.5, 71.4, 68.8, 67.7, 61.0, 50.0, 47.3. ^{19}F NMR (378 MHz, DMSO-d_6): δ −62.8. HRMS (ESI+): m/z calcd for $C_{29}H_{32}N_{12}O_{11}SF_3$ $[M+H]^+$: 813.1986, Found 813.1988.

4.1.33. N-{[(2R,5R)-5-(6-amino-9H-purin-9-yl)-3,4-dihydroxyoxolan-2-yl]methyl}-N-(2-{[(2R,5R)-2-(6-amino-9H-purin-9-yl)-4-hydroxy-5-(hydroxymethyl)oxolan-3-yl]oxy}ethyl)-4-chloro-3-nitrobenzene-1-sulfonamide (13)

Using **method C** with **33** (121 mg, 0.12 mmol, 1.00 eq) and a 0–40% linear gradient of acetonitrile in TEAAc buffer 50 mM, pH 7 for purification, **13** (14 mg, 16%) was obtained as a white powder with 98% purity determined by HPLC analysis at 260 nm. ^{1}H NMR (500 MHz, DMSO-d_6) δ 8.42 (d, J = 2.2 Hz, 1H), 8.34 (s, 1H), 8.32 (s, 1H), 8.144 (s, 1H), 8.140 (s, 1H), 7.96 (dd, J = 8.5 Hz, J = 2.2 Hz, 1H), 7.77 (d, J = 8.5 Hz, 1H), 7.41 (br. s, 2H) 7.35 (br. s, 2H), 5.90 (d, J = 5.2 Hz, 1H), 5.83 (d, J = 5.8 Hz, 1H), 5.59 (d, J = 6.0 Hz, 1H), 5.48–5.31 (m, 2H), 5.25 (d, J = 5.3 Hz, 1H), 4.72 (q, J = 5.5 Hz, 1H), 4.36 (t, J = 5.0 Hz, 1H), 4.29 (q, J = 4.6 Hz, 1H), 4.22–4.08 (m, 2H), 3.87 (q, J = 3.6 Hz, 1H), 3.78–3.70 (m, 2H), 3.67 (dd, J = 12.2 Hz, J = 3.4 Hz, 1H), 3.56–3.29 (m, 5H). ^{13}C NMR (125 MHz, DMSO-d_6) δ 156.1, 156.0, 152.6, 152.5, 149.3, 148.9, 147.4, 140.1, 139.5, 139.5, 132.7, 131.6, 129.6, 124.3, 119.3, 119.3, 87.6, 86.2, 85.8, 81.8, 81.5, 72.3, 71.3, 68.8, 68.1, 61.4, 50.8, 48.1. HRMS (ESI+): m/z calcd for $C_{28}H_{32}N_{12}O_{11}SCl$ $[M+H]^+$: 779.1723, Found 779.1730.

4.1.34. N-{[(4R,6R)-6-(6-amino-9H-purin-9-yl)-2,2-dimethyl-tetrahydro-2H-furo[3,4-d] [1,3]dioxol-4-yl]methyl}-N-(2-{[(2R,5R)-2-(6-amino-9H-purin-9-yl)-4-[(tert-butyldimethylsilyl)oxy]-5-{[(tert-butyldimethylsilyl)oxy]methyl}oxolan-3-yl]oxy}ethyl)-4-chlorobenzene-1-sulfonamide (34)

To a solution of **20** (171 mg, 0.21 mmol, 1.00 eq) in anhydrous DCM (2 mL) was added Et_3N (60 μL, 0.41 mmol, 2.00 eq). 4-chlorobenzenesulfonyl chloride (65 mg, 0.31 mmol, 1.50 eq) was added at 0 °C and the reaction mixture was stirred for 3 h at room temperature under argon. Solvents were removed under vacuum and the residue was diluted with DCM (40 mL) and washed with saturated aqueous $NaHCO_3$ (40 mL). The aqueous layer was extracted with DCM (3 × 30 mL) and the combined organic extracts were washed with brine (30 mL), dried over Na_2SO_4 and concentrated under vacuum. The residue was purified by flash column chromatography (silica gel, linear gradient 0–4% MeOH in DCM) to give **34** (188 mg, 90%) as a white solid. R_f 0.67 (10:90 MeOH/CH_2Cl_2). ^{1}H NMR (500 MHz, $CDCl_3$) δ 8.32 (s, 1H), 8.29 (s, 1H), 8.12 (s, 1H), 7.81 (s, 1H), 7.59–7.46 (m, 2H), 7.34–7.22 (m, 2H), 5.97 (d, J = 3.3 Hz, 1H), 5.96–5.88 (m, 5H), 5.41 (dd, J = 6.4 Hz, J = 2.0 Hz, 1H), 5.07 (dd, J = 6.4 Hz, J = 3.5 Hz, 1H), 4.50 (dd, J = 5.9 Hz, J = 4.6 Hz, 1H), 4.46–4.34 (m, 1H), 4.21 (dd, J = 4.7 Hz, J = 3.3 Hz, 1H), 4.03 (dt, J = 6.0 Hz, J = 3.0 Hz, 1H), 3.98 (dd, J = 11.4 Hz, J = 3.5 Hz, 1H), 3.80–3.72 (m, 3H), 3.68 (dd, J = 14.6 Hz, J = 5.6 Hz, 1H), 3.46–3.31 (m, 3H), 1.57 (s, 3H), 1.36 (s, 3H), 0.91 (s, 9H), 0.89 (s, 9H), 0.11–0.03 (m, 12H). ^{13}C NMR (125 MHz, $CDCl_3$) δ 155.8, 155.6, 153.2, 153.1, 149.5, 149.1, 140.2, 139.5, 139.1, 138.0, 129.2, 128.6, 120.5, 120.2, 114.6, 90.9, 87.3, 85.3, 84.5, 84.1, 82.6 (2C), 69.6 (2C), 61.6, 50.7, 48.1, 27.2, 26.1, 25.9, 25.4, 18.6, 18.2, −4.5, −4.7, −5.3. HRMS (ESI+): m/z calcd for $C_{43}H_{65}N_{11}O_9SSi_2Cl$ $[M+H]^+$: 1002.3909, found: 1002.3928.

4.1.35. 9-[(2R,5R)-3-[2-({[(4R,6R)-6-(6-amino-9H-purin-9-yl)-2,2-dimethyl-tetrahydro-2H-furo[3,4-d] [1,3]dioxol-4-yl]methyl}[(4-chloro-3-nitrophenyl)methyl]amino)ethoxy]-4-[(tert-butyldimethylsilyl)oxy]-5-{[(tert-butyldimethylsilyl)oxy]methyl} oxolan-2-yl]-9H-purin-6-amine (35)

To a solution of **20** (100 mg, 0.12 mmol, 1.00 eq) in anhydrous DCE (3.5 mL) was added a solution of 4-chloro-3-nitrobenazaldehyde (27 mg, 0.18 mmol, 1.50 eq) in anhydrous DCE (3.5 mL) and acetic acid (10 μL, 0.18 mmol, 1.50 eq). After stirring for 20 min at 40 °C under argon, sodium triacetoxyborohydride (38 mg, 0.18 mmol, 1.50 eq) was added. After stirring at 40 °C for 16 h, the solution was diluted with DCM (30 mL) and washed with saturated aqueous $NaHCO_3$. The aqueous layer was extracted with DCM (3 × 30 mL) and the combined organic extracts were washed with brine (60 mL), dried over Na_2SO_4 and concentrated under vacuum. The residue was purified by flash column chromatography (silica gel, linear gradient 0–5% MeOH in DCM) to give **35** as a white solid (105 mg, 87%). R_f 0.71 (MeOH/DCM 5:95). ^{1}H NMR (500 MHz, $CDCl_3$) δ 8.27 (s, 1H), 8.18 (s, 1H), 8.15 (s, 1H), 7.82 (br. s, 2H), 7.29–7.27 (m, 2H), 6.22 (br. s, 2H), 6.20 (br. s, 2H), 6.10 (d, J = 3.6 Hz, 1H), 5.99 (d, J = 2.1 Hz, 1H), 5.37 (dd, J = 6.5 Hz, J = 2.1 Hz, 1H), 4.91 (dd, J = 6.5 Hz, J = 3.7 Hz, 1H), 4.48 (t, J = 5.1 Hz, 1H), 4.30 (td, J = 6.7 Hz, J = 3.6 Hz, 1H), 4.22 (t, J = 4.2 Hz, 1H), 4.07 (dt, J = 5.8 Hz, J = 3.0 Hz, 1H), 3.99 (dd, J = 11.5 Hz, J = 3.4 Hz, 1H), 3.81–3.72 (m, 2H), 3.71–3.66 (m, 1H), 3.65–3.61 (m, 2H), 2.90–2.70 (m, 4H), 1.57 (s, 3H), 1.36 (s, 3H), 0.92 (s, 9H), 0.86 (s, 9H), 0.14 – - 0.02 (m, 12H). ^{13}C NMR (125 MHz, $CDCl_3$) δ 155.8, 155.7, 153.1, 153.0, 149.6, 149.0, 147.8, 140.6, 140.1, 139.3, 133.0, 131.4, 125.6, 125.2, 120.3, 120.1, 114.6, 90.8, 87.0, 85.7, 84.9, 84.0, 83.4, 82.8, 69.6, 69.3, 61.8, 58.2, 56.4, 53.5, 27.2, 26.2, 25.8, 25.4, 18.6, 18.2, −4.5, −4.7, −5.2, −5.3. HRMS (ESI+): m/z calcd for $C_{44}H_{66}N_{12}O_9Si_2Cl$ $[M+H]^+$: 997.4297, found: 997.4327.

4.1.36. 9-[(2R,5R)-3-[2-({[(4R,6R)-6-(6-amino-9H-purin-9-yl)-2,2-dimethyl-tetrahydro-2H-furo[3,4-d] [1,3]dioxol-4-yl]methyl}[(4-chlorophenyl)methyl]amino)ethoxy]-4-[(tert-butyldimethylsilyl) oxy]-5-{[(tert-butyldimethylsilyl)oxy]methyl}oxolan-2-yl]-9H-purin-6-amine (36)

To a solution of **20** (210 mg, 0.25 mmol, 1.00 eq) in anhydrous DCE (7 mL) was added 4-chlorobenzaldehyde (43 mg, 0.38 mmol, 1.50 eq) in anhydrous DCE (7 mL) and acetic acid (18 μL, 0.38 mmol, 1.50 eq). After stirring for 20 min at 40 °C under argon, sodium triacetoxyborohydride (81 mg, 0.38 mmol, 1.50 eq) was added. After stirring at 40 °C for 16 h, the solution was diluted with DCM (50 mL) and washed with saturated aqueous $NaHCO_3$. The aqueous layer was extracted with DCM (3 × 50 mL) and the combined organic extracts were washed with brine (70 mL), dried over Na_2SO_4 and concentrated under vacuum. The residue was purified by flash column chromatography (silica gel, linear gradient 0–5% MeOH in DCM) to give **36** as a white solid (172 mg, 0.18 mmol, 72%). R_f 0.71 (MeOH/CH_2Cl_2 5:95). ^{1}H NMR (600 MHz, $CDCl_3$) δ 8.30 (s, 1H), 8.20 (s, 1H), 8.15 (s, 1H), 7.83 (s, 1H), 7.19–7.07 (m, 4H), 6.11 (d, *J* = 3.7 Hz, 1H), 5.99 (d, *J* = 2.2 Hz, 1H), 5.97–5.83 (m, 4H), 5.37 (dd, *J* = 6.5 Hz, *J* = 2.2 Hz, 1H), 4.85 (dd, *J* = 6.4 Hz, *J* = 3.4 Hz, 1H), 4.49 (t, *J* = 5.1 Hz, 1H), 4.32 (td, *J* = 6.7 Hz, *J* = 3.3 Hz, 1H), 4.26 (t, *J* = 4.2 Hz, 1H), 4.08 (dt, *J* = 5.9 Hz, *J* = 3.1 Hz, 1H), 3.98 (dd, *J* = 11.5 Hz, *J* = 3.6 Hz, 1H), 3.79–3.47 (m, 5H), 2.84–2.66 (m, 4H), 1.58 (s, 3H), 1.36 (s, 3H), 0.92 (s, 9H), 0.88 (s, 9H), 0.13–0.02 (m, 12H). ^{13}C NMR (150 MHz, $CDCl_3$) δ 155.7, 155.6, 153.1, 153.1, 149.7, 149.3, 140.0, 139.5, 137.8, 132.8, 130.1, 128.4, 120.5, 120.3, 114.4, 91.0, 87.2, 85.7, 84.9, 84.0, 83.5, 82.7, 69.8, 69.5, 61.3, 58.6, 56.4, 53.6, 27.3, 26.2, 25.9, 25.5, 18.6, 18.2, −4.5, −4.7, −5.2, −5.3. HRMS (ESI+): *m/z* calcd for $C_{44}H_{67}N_{11}O_7Si_2Cl$ $[M+H]^+$: 952.4447, found: 952.4426.

4.1.37. N-{[(2R,5R)-5-(6-amino-9H-purin-9-yl)-3,4-dihydroxyoxolan-2-yl]methyl}-N-(2-{[(2R,5R)-2-(6-amino-9H-purin-9-yl)-4-hydroxy-5-(hydroxymethyl)oxolan-3-yl]oxy}ethyl)-4-chlorobenzene-1-sulfonamide (14)

Using **method C** with **34** (150 mg, 0.15 mmol, 1.00 eq) and a 0–40% linear gradient of acetonitrile in TEAAc buffer 50 mM, pH 7 for purification, **14** (55 mg, 48%) was obtained as a white powder with 96% purity determined by HPLC analysis at 260 nm. ^{1}H NMR (600 MHz, DMSO-d_6) δ 8.33 (s, 1H), 8.32 (s, 1H), 8.150 (s, 1H), 8.147 (s, 1H), 7.75–7.68 (m, 2H), 7.53–7.49 (m, 2H), 7.35 (br. s, 2H), 7.28 (br. s, 2H), 5.95 (d, *J* = 5.5 Hz, 1H), 5.84 (d, *J* = 5.9 Hz, 1H), 5.52 (d, *J* = 6.1 Hz, 1H), 5.36 (m, 2H), 5.20 (d, *J* = 5.2 Hz, 1H), 4.74 (q, *J* = 5.6 Hz, 1H), 4.39 (t, *J* = 5.2 Hz, 1H), 4.29 (q, *J* = 4.7 Hz, 1H), 4.16 (q, *J* = 4.6 Hz, 1H), 4.11–4.05 (m, 1H), 3.93 (q, *J* = 3.6 Hz, 1H), 3.73–3.64 (m, 3H), 3.56–3.46 (m, 2H), 3.37–3.29 (m, 3H), 3.22 (dt, *J* = 14.7 Hz, 6.4 Hz, 1H). ^{13}C NMR (150 MHz, DMSO-d_6) δ 156.1, 156.0, 152.5, 152.5, 149.3, 148.9, 140.1, 139.5, 138.0, 137.7, 129.2, 128.7, 119.3, 119.3, 87.7, 86.2, 85.9, 82.1, 81.4, 72.2, 71.3, 69.9, 68.3, 61.1, 50.8, 47.7. HRMS (ESI+): *m/z* calcd for $C_{28}H_{33}N_{11}O_9SCl$ $[M+H]^+$: 734.1868, Found 734.1866.

4.1.38. (2R,5R)-2-(6-amino-9H-purin-9-yl)-5-{[(2-{[(2R,5R)-2-(6-amino-9H-purin-9-yl)-4-hydroxy-5-(hydroxymethyl)oxolan-3-yl]oxy}ethyl)[(4-chloro-3-nitrophenyl)methyl]amino]methyl}oxolane-3,4-diol (15)

Using **method C** with **35** (140 mg, 0.14 mmol, 1.00 eq) and a 0–40% linear gradient of acetonitrile in TEAAc buffer 50 mM, pH 7 for purification, **15** (25 mg, 25%) was obtained as a white powder with 99% purity determined by HPLC analysis at 260 nm. ^{1}H NMR (600 MHz, DMSO-d_6) δ 8.35 (s, 1H), 8.23 (s, 1H), 8.11 (s, 1H), 8.07 (s, 1H), 7.89 (d, *J* = 1.9 Hz, 1H), 7.50 (d, *J* = 8.3 Hz, 1H), 7.45 (dd, *J* = 8.3 Hz, *J* = 2.0 Hz, 1H), 7.32 (br. s, 2H), 7.24 (br. s, 2H), 5.99 (d, *J* = 5.9 Hz, 1H), 5.83 (d, *J* = 5.1 Hz, 1H), 5.51–5.32 (m, 2H), 5.24 (br. s, 1H), 5.13 (br. s, 1H), 4.57 (t, *J* = 5.2 Hz, 1H), 4.45 (dd, *J* = 6.1 Hz, *J* = 4.8 Hz, 1H), 4.30 (t, *J* = 4.1 Hz, 1H), 4.05 (t, *J* = 5.0 Hz, 1H), 4.02–3.95 (m, 2H), 3.73–3.63 (m, 4H), 3.58–3.51 (m, 2H), 2.83 (dd, *J* = 14.0 Hz, *J* = 4.4 Hz, 1H), 2.73 (dd, *J* = 14.0 Hz, *J* = 7.2 Hz, 1H), 2.69–2.63 (m, 2H). ^{13}C NMR (150 MHz, DMSO-d_6) δ 156.1, 156.0, 152.5 (2C), 149.3, 148.9, 147.2, 140.1, 139.8, 139.6, 133.7, 131.0, 125.0, 122.9, 119.3, 119.2, 87.8, 86.2, 86.1, 82.2, 81.3, 72.4, 71.8, 68.9, 68.1, 61.3, 56.8, 56.0, 53.0. HRMS (ESI+): *m/z* calcd for $C_{29}H_{34}N_{12}O_9Cl$ $[M+H]^+$: 729.2255, Found 729.2256.

4.1.39. (2R,5R)-2-(6-amino-9H-purin-9-yl)-5-{[(2-{[(2R,5R)-2-(6-amino-9H-purin-9-yl)-4-hydroxy-5-(hydroxymethyl)oxolan-3-yl]oxy}ethyl)[(4-chlorophenyl)methyl]amino]methyl}oxolane-3,4-diol (16)

Using **method C** with **36** (172 mg, 0.18 mmol, 1.00 eq) and a 0–40% linear gradient of acetonitrile in TEAAc buffer 50 mM, pH 7 for purification, **16** (45 mg, 37%) was obtained as a white powder with 98% purity determined by HPLC analysis at 260 nm. ^{1}H NMR (600 MHz, DMSO-d_6) δ 8.36 (s, 1H), 8.25 (s, 1H), 8.13 (s, 1H), 8.11 (s, 1H), 7.34 (br. s, 2H), 7.25 (br. s, 2H), 7.23–7.17 (m, 2H), 7.17–7.11 (m, 2H), 6.00 (d, *J* = 6.2 Hz, 1H), 5.84 (d, *J* = 5.0 Hz, 1H), 5.45–5.39 (m, 2H), 5.27 (d, *J* = 4.8 Hz, 1H), 5.12 (d, *J* = 5.4 Hz, 1H), 4.58 (q, *J* = 5.5 Hz, 1H), 4.48 (dd, *J* = 6.2 Hz, *J* = 4.8 Hz, 1H), 4.30 (td, *J* = 4.6 Hz, *J* = 2.9 Hz, 1H), 4.04 (q, *J* = 5.1 Hz, 1H), 4.02–3.96 (m, 2H), 3.70–3.63 (m, 2H), 3.60–3.48 (m, 4H), 2.80 (dd, *J* = 14.0 Hz, *J* = 4.5 Hz, 1H), 2.67 (dd, *J* = 13.9 Hz, *J* = 7.0 Hz, 1H), 2.61 (q, *J* = 6.1 Hz, 2H). ^{13}C NMR (150 MHz, DMSO-d_6) δ 156.2, 156.0, 152.6, 152.5, 149.3, 149.0, 139.8, 139.7, 138.2, 131.1, 130.4, 127.8, 119.3, 119.16, 87.67, 86.3, 86.1, 82.4, 81.2, 72.4, 71.8, 69.0, 67.5, 61.5, 57.5, 55.8, 52.9. HRMS (ESI+): *m/z* calcd for $C_{29}H_{35}N_{11}O_7Cl$ $[M+H]^+$: 684.2404, Found 684.2398.

4.2. Expression and purification of recombinant proteins

SARS-CoV nsp14 and human RNA N7-methyltransferase (hRNMT) coding sequences were cloned in fusion with a N-terminus hexa-histidine tag in Gateway® plasmids. The proteins were expressed in *E. coli* and purified following previously described protocols [33,39]. Vaccinia virus capping enzyme (D1/D12 complex) and mRNA Cap 2′-*O*-methyltransferase (VP39) were purchased (New England Biolabs).

4.3. MTase filter binding assay (FBA)

The transfer of tritiated methyl from [^{3}H] SAM onto RNA substrate was monitored by filter binding assay, performed according to the method described previously [40]. Assays were carried out in reaction mixture [40 mM Tris-HCl (pH 8.0), 1 mM DTT, 1 mM $MgCl_2$, 2 μM SAM and 0.1 μM ^{3}H-SAM (PerkinElmer)] in the presence of 0.7 μM $GpppAC_4$ synthetic RNA and SARS-CoV nsp14 (50 nM), vaccinia virus capping enzyme (D1-D12) (41 U), or human RNA N7 MTase (hRNMT) (50 nM). The enzymes were first mixed with compounds suspended in 100% DMSO (5% final DMSO) before the addition of RNA substrate and SAM and then incubated at 30 °C. Control reactions were performed in the presence of 5% DMSO. Reactions mixtures were stopped after 30 min by their 10-fold dilution in ice-cold water. Samples were transferred to diethylaminoethyl (DEAE) filtermat (PerkinElmer) using a Filtermat Harvester (Packard Instruments). The RNA-retaining mats were washed twice with 10 mM ammonium formate pH 8.0, twice with water and once with ethanol. They were soaked with scintillation fluid (PerkinElmer), and ^{3}H-methyl transfer to the RNA substrates was determined using a Wallac MicroBeta TriLux Liquid Scintillation Counter (PerkinElmer). For IC_{50} measurements, values were normalized and fitted with Prism (GraphPad software) using the following equation: Y = 100/(1+((X/IC_{50})^Hillslope)). IC_{50} is

defined as the inhibitory compound concentration that causes 50% reduction in enzyme activity.

4.4. Differential scanning fluorimetry (DSF)

The thermal stabilization of the native protein structure upon ligand binding was monitored by differential scanning fluorimetry, performed according to the method described previously [34] with some modifications. Reaction mixture (25 μL) consisted of 20 mM HEPES (pH 7.5), 150 mM NaCl, 1X SYPRO orange dye (Invitrogen), 5 μM SARS-CoV nsp14 protein and 1 mM compound previously dissolved in 100% DMSO or water (SAM and Sinefungin). The protein was first mixed with compound before the addition of the dye and incubated in 96-well white microplates (Bio-Rad). Fluorescence intensities were measured from 20 to 95 °C with a ramp rate of 0.2 °C/min using a Real-Time PCR detection system (Bio-Rad). Control reactions were performed in the presence of 5% DMSO. Fluorescence intensities were plotted as a function of temperature and melting temperature (T_m) was determined by curve-fitting using Prism (GraphPad software). The apparent affinity constant (K_D) for compound **13** was calculated by nonlinear regression analysis with one site-specific binding equation Hill slope using Prism (GraphPad software).

4.5. Molecular docking

All calculations were performed using Autodock vina (The Scripps Research Institute, La Jolla, CA) on a MSI computer with a 2.30 GHz Intel Core i5-8300H. The solved X-ray crystal structure of SARS-CoV nsp14 (PDB 5C8T) was used as a static receptor for docking. Both the co-crystalized ligand SAM and ions were removed from the SARS-CoV nsp14 protein using VMD 1.9.3 software. The ligand structures were drawn and minimized using MarvinSketch (ChemAxon). Targeted protein and ligand structures with polar hydrogens were converted to the required PDBQT format using MGL Tools (version 1.5.6). The docking was performed with a search box located at $x = -11.155$, $y = -40.77$, $z = -3.688$ coordinates, with a search box size of $25 \times 25 \times 25$ Å3. After calculations, PDB files were analyzed using Pymol (version 2.3).

4.6. Accession codes

PDB code for SARS-CoV nsp14 bound SAM is 5C8T. PDB code for SARS-CoV nsp14 is 5NFY.

Author contributions

All authors have contributed to the manuscript and given approval to the final version of the manuscript.

Declaration of competing interest

The authors declare that they have no known competing financial interests or personal relationships that could have appeared to influence the work reported in this paper.

Acknowledgments

Rostom Ahmed-Belkacem acknowledges University of Montpellier for the financial support of his PhD work.

Appendix A. Supplementary data

Supplementary data to this article can be found online at https://doi.org/10.1016/j.ejmech.2020.112557.

References

[1] J.M. Shultz, Z. Espinel, M. Espinola, A. Rechkemmer, Distinguishing epidemiological features of the 2013-2016 West Africa Ebola virus disease outbreak, Disaster Health 3 (2016) 78–88, https://doi.org/10.1080/21665044.2016.1228326.

[2] P.A. Rota, M.S. Oberste, S.S. Monroe, W.A. Nix, R. Campagnoli, J.P. Icenogle, S. Penaranda, B. Bankamp, K. Maher, M.H. Chen, S. Tong, A. Tamin, L. Lowe, M. Frace, J.L. DeRisi, Q. Chen, D. Wang, D.D. Erdman, T.C. Peret, C. Burns, T.G. Ksiazek, P.E. Rollin, A. Sanchez, S. Liffick, B. Holloway, J. Limor, K. McCaustland, M. Olsen-Rasmussen, R. Fouchier, S. Gunther, A.D. Osterhaus, C. Drosten, M.A. Pallansch, L.J. Anderson, W.J. Bellini, Characterization of a novel coronavirus associated with severe acute respiratory syndrome, Science 300 (2003) 1394–1399, https://doi.org/10.1126/science.1085952.

[3] E. de Wit, N. van Doremalen, D. Falzarano, V.J. Munster, SARS and MERS: recent insights into emerging coronaviruses, Nat. Rev. Microbiol. 14 (2016) 523–534, https://doi.org/10.1038/nrmicro.2016.81.

[4] F. Wu, S. Zhao, B. Yu, Y.-M. Chen, W. Wang, Z.-G. Song, Y. Hu, Z.-W. Tao, J.-H. Tian, Y.-Y. Pei, M.-L. Yuan, Y.-L. Zhang, F.-H. Dai, Y. Liu, Q.-M. Wang, J.-J. Zheng, L. Xu, E.C. Holmes, Y.-Z. Zhang, A new coronavirus associated with human respiratory disease in China, Nature 579 (2020) 265–269, https://doi.org/10.1038/s41586-020-2008-3.

[5] P. Zhou, X.-L. Yang, X.-G. Wang, B. Hu, L. Zhang, W. Zhang, H.-R. Si, Y. Zhu, B. Li, C.-L. Huang, H.-D. Chen, J. Chen, Y. Luo, H. Guo, R.-D. Jiang, M.-Q. Liu, Y. Chen, X.-R. Shen, X. Wang, X.-S. Zheng, K. Zhao, Q.-J. Chen, F. Deng, L.-L. Liu, B. Yan, F.-X. Zhan, Y.-Y. Wang, G.-F. Xiao, Z.-L. Shi, A pneumonia outbreak associated with a new coronavirus of probable bat origin, Nature 579 (2020) 270–273, https://doi.org/10.1038/s41586-020-2012-7.

[6] C. Huang, Y. Wang, X. Li, L. Ren, J. Zhao, Y. Hu, L. Zhang, G. Fan, J. Xu, X. Gu, Z. Cheng, T. Yu, J. Xia, Y. Wei, W. Wu, X. Xie, W. Yin, H. Li, M. Liu, Y. Xiao, H. Gao, L. Guo, J. Xie, G. Wang, R. Jiang, Z. Gao, Q. Jin, J. Wang, B. Cao, Clinical features of patients infected with 2019 novel coronavirus in Wuhan, China, Lancet 395 (2020) 497–506, https://doi.org/10.1016/S0140-6736(20)30183-5.

[7] WHO, Coronavirus Disease (COVID-19) Outbreak Situation, 2020. https://www.who.int/emergencies/diseases/novel-coronavirus-2019, 5.

[8] E. Decroly, B. Canard, Biochemical principles and inhibitors to interfere with viral capping pathways, Curr. Opin. Virol. 24 (2017) 87–96, https://doi.org/10.1016/j.coviro.2017.04.003.

[9] M. Becares, A. Pascual-Iglesias, A. Nogales, I. Sola, L. Enjuanes, S. Zuñiga, Mutagenesis of coronavirus nsp14 reveals its potential role in modulation of the innate immune response, J. Virol. 90 (2016) 5399–5414, https://doi.org/10.1128/jvi.03259-15.

[10] Y. Sun, Z. Wang, J. Tao, Y. Wang, A. Wu, Z. Yang, K. Wang, L. Shi, Y. Chen, D. Guo, Yeast-based assays for the high-throughput screening of inhibitors of coronavirus RNA cap guanine-N7-methyltransferase, Antivir. Res. 104 (2014) 156–164, https://doi.org/10.1016/j.antiviral.2014.02.002.

[11] W. Aouadi, C. Eydoux, B. Coutard, B. Martin, F. Debart, J.J. Vasseur, J.M. Contreras, C. Morice, G. Quérat, M.-L. Jung, B. Canard, J.-C. Guillemot, E. Decroly, Toward the identification of viral cap-methyltransferase inhibitors by fluorescence screening assay, Antivir. Res. 144 (2017) 330–339, https://doi.org/10.1016/j.antiviral.2017.06.021.

[12] J. Zhang, Y.G. Zheng, SAM/SAH analogs as versatile tools for SAM-dependent methyltransferases, ACS Chem. Biol. 11 (2016) 583–597, https://doi.org/10.1021/acschembio.5b00812.

[13] R. Gana, S. Rao, H. Huang, C. Wu, S. Vasudevan, Structural and functional studies of S-adenosyl-L-methionine binding proteins: a ligand-centric approach, BMC Struct. Biol. 13 (2013) 6, https://doi.org/10.1186/1472-6807-13-6.

[14] R. Ahmed-Belkacem, P. Sutto-Ortiz, E. Decroly, J.-J. Vasseur, F. Debart, Synthesis of adenine dinucleosides 2′,5′-bridged by sulfur-containing linkers as bisubstrate SAM analogues for viral RNA 2′-O-methyltransferases, Eur. J. Org Chem. (2019) 6486–6495, https://doi.org/10.1002/ejoc.201901120.

[15] L. Halby, N. Marechal, D. Pechalrieu, V. Cura, D.-M. Franchini, C. Faux, F. Alby, N. Troffer-Charlier, S. Kudithipudi, A. Jeltsch, W. Aouadi, E. Decroly, J.-C. Guillemot, P. Page, C. Ferroud, L. Bonnefond, D. Guianvarc'h, J. Cavarelli, B. Arimondo Paola, Hijacking DNA methyltransferase transition state analogues to produce chemical scaffolds for PRMT inhibitors, Philos. Trans. R. Soc. London, Ser. A B 373 (2018) 20170072, https://doi.org/10.1098/rstb.2017.0072.

[16] C. Atdjian, L. Iannazzo, E. Braud, M. Ethève-Quelquejeu, Synthesis of SAM-adenosine conjugates for the study of m6A-RNA methyltransferases, Eur. J. Org Chem. (2018) 4411–4425, https://doi.org/10.1002/ejoc.201800798.

[17] S. Oerum, M. Catala, C. Atdjian, F. Brachet, L. Ponchon, P. Barraud, L. Iannazzo, L. Droogmans, E. Braud, M. Ethève-Quelquejeu, C. Tisné, Bisubstrate analogues as structural tools to investigate m6A methyltransferase active sites, RNA Biol. (2019) 1–11, https://doi.org/10.1080/15476286.2019.1589360.

[18] S. Srinivasan, H. Cui, Z. Gao, M. Liu, S. Lu, W. Mkandawire, O. Narykov, M. Sun, D. Korkin, Structural genomics of SARS-CoV-2 indicates evolutionary conserved functional regions of viral proteins, Viruses 12 (2020) 360, https://doi.org/10.3390/v12040360.

[19] Y.-Y. Ku, V.S. Chan, A. Christesen, T. Grieme, M. Mulhern, Y.-M. Pu, M.D. Wendt, Development of a convergent large-scale synthesis for venetoclax, a first-in-class BCL-2 selective inhibitor, J. Org. Chem. 84 (2019) 4814–4829, https://doi.org/10.1021/acs.joc.8b02750.

[20] Y. Yu, Tazeem, Z. Xu, L. Du, M. Jin, C. Dong, H.-B. Zhou, S. Wu, Design and synthesis of heteroaromatic-based benzenesulfonamide derivatives as potent inhibitors of H5N1 influenza A virus, MedChemComm 10 (2019) 89–100, https://doi.org/10.1039/C8MD00474A.
[21] Y. Yao, P. Chen, J. Diao, G. Cheng, L. Deng, J.L. Anglin, B.V.V. Prasad, Y. Song, Selective inhibitors of histone methyltransferase DOT1L: design, synthesis, and crystallographic studies, J. Am. Chem. Soc. 133 (2011) 16746–16749, https://doi.org/10.1021/ja206312b.
[22] T. Kan, T. Fukuyama, Ns strategies: a highly versatile synthetic method for amines, Chem. Commun. (2004) 353–359, https://doi.org/10.1039/B311203A.
[23] M. Kolb, C. Danzin, J. Barth, N. Claverie, Synthesis and biochemical properties of chemically stable product analogs of the reaction catalyzed by S-adenosyl-L-methionine decarboxylase, J. Med. Chem. 25 (1982) 550–556, https://doi.org/10.1021/jm00347a014.
[24] X.-H. Pan, P. Jiang, Z.-H. Jia, K. Xu, J. Cao, C. Chen, M.-H. Shen, H.-D. Xu, Expedient catalytic construction of azabicyclo[4.1.0]/[5.1.0] carbaldehydes via intramolecular cyclopropanation, Tetrahedron 71 (2015) 5124–5129, https://doi.org/10.1016/j.tet.2015.05.113.
[25] A.J. Mitchell, N.P. Dunham, R.J. Martinie, J.A. Bergman, C.J. Pollock, K. Hu, B.D. Allen, W.-c. Chang, A. Silakov, J.M. Bollinger, C. Krebs, A.K. Boal, Visualizing the reaction cycle in an iron(ii)- and 2-(oxo)-glutarate-dependent hydroxylase, J. Am. Chem. Soc. 139 (2017) 13830–13836, https://doi.org/10.1021/jacs.7b07374.
[26] A.F. Abdel-Magid, S.J. Mehrman, A review on the use of sodium triacetoxyborohydride in the reductive amination of ketones and aldehydes, Org. Process Res. Dev. 10 (2006) 971–1031, https://doi.org/10.1021/op0601013.
[27] S. Iwaki, K. Hanaoka, W. Piao, T. Komatsu, T. Ueno, T. Terai, T. Nagano, Development of hypoxia-sensitive Gd^{3+}-based MRI contrast agents, Bioorg. Med. Chem. Lett 22 (2012) 2798–2802, https://doi.org/10.1016/j.bmcl.2012.02.071.
[28] L. Devisscher, S. Van Coillie, S. Hofmans, D. Van Rompaey, K. Goossens, E. Meul, L. Maes, H. De Winter, P. Van Der Veken, P. Vandenabeele, T.V. Berghe, K. Augustyns, Discovery of novel, drug-like ferroptosis inhibitors with in vivo efficacy, J. Med. Chem. 61 (2018) 10126–10140, https://doi.org/10.1021/acs.jmedchem.8b01299.
[29] R.J. Cherney, J.J.W. Duan, M.E. Voss, L. Chen, L. Wang, D.T. Meyer, Z.R. Wasserman, K.D. Hardman, R.-Q. Liu, M.B. Covington, M. Qian, S. Mandlekar, D.D. Christ, J.M. Trzaskos, R.C. Newton, R.L. Magolda, R.R. Wexler, C.P. Decicco, Design, synthesis, and evaluation of benzothiadiazepine hydroxamates as selective tumor necrosis factor-α converting enzyme inhibitors, J. Med. Chem. 46 (2003) 1811–1823, https://doi.org/10.1021/jm020475w.
[30] T.A. Moss, D.M. Barber, A.F. Kyle, D.J. Dixon, Catalytic asymmetric alkylation reactions for the construction of protected ethylene-amino and propylene-amino motifs attached to quaternary stereocentres, Chem. Eur J. 19 (2013) 3071–3081, https://doi.org/10.1002/chem.201203825.
[31] A. Salahuddin, A. Inam, R.L. van Zyl, D.C. Heslop, C.-T. Chen, F. Avecilla, S.M. Agarwal, A. Azam, Synthesis and evaluation of 7-chloro-4-(piperazin-1-yl)quinoline-sulfonamide as hybrid antiprotozoal agents, Biorg. Med. Chem. 21 (2013) 3080–3089, https://doi.org/10.1016/j.bmc.2013.03.052.
[32] A. Vermote, G. Brackman, M.D.P. Risseeuw, T. Coenye, S. Van Calenbergh, Design, synthesis and biological evaluation of novel hamamelitannin analogues as potentiators for vancomycin in the treatment of biofilm related staphylococcus aureus infections, Biorg. Med. Chem. 24 (2016) 4563–4575, https://doi.org/10.1016/j.bmc.2016.07.058.
[33] F. Peyrane, B. Selisko, E. Decroly, J.J. Vasseur, D. Benarroch, B. Canard, K. Alvarez, High-yield production of short GpppA- and 7^{me}GpppA-capped RNAs and HPLC-monitoring of methyltransfer reactions at the guanine-N7 and adenosine-2'O positions, Nucleic Acids Res. 35 (2007) e26, https://doi.org/10.1093/nar/gkl1119.
[34] F.H. Niesen, H. Berglund, M. Vedadi, The use of differential scanning fluorimetry to detect ligand interactions that promote protein stability, Nat. Protoc. 2 (2007) 2212–2221, https://doi.org/10.1038/nprot.2007.321.
[35] Y. Ma, L. Wu, N. Shaw, Y. Gao, J. Wang, Y. Sun, Z. Lou, L. Yan, R. Zhang, Z. Rao, Structural basis and functional analysis of the SARS coronavirus nsp14-nsp10 complex, Proc. Natl. Acad. Sci. U. S. A. 112 (2015) 9436–9441, https://doi.org/10.1073/pnas.1508686112.
[36] F. Ferron, L. Subissi, A.T. Silveira De Morais, N.T.T. Le, M. Sevajol, L. Gluais, E. Decroly, C. Vonrhein, G. Bricogne, B. Canard, I. Imbert, Structural and molecular basis of mismatch correction and ribavirin excision from coronavirus RNA, Proc. Natl. Acad. Sci. U. S. A. 115 (2018) e162–e171, https://doi.org/10.1073/pnas.1718806115.
[37] P. Auffinger, F.A. Hays, E. Westhof, P.S. Ho, Halogen bonds in biological molecules, Proc. Natl. Acad. Sci. U. S. A. 101 (2004) 16789–16794, https://doi.org/10.1073/pnas.0407607101.
[38] R. Lu, X. Zhao, J. Li, P. Niu, B. Yang, H. Wu, W. Wang, H. Song, B. Huang, N. Zhu, Y. Bi, X. Ma, F. Zhan, L. Wang, T. Hu, H. Zhou, Z. Hu, W. Zhou, L. Zhao, J. Chen, Y. Meng, J. Wang, Y. Lin, J. Yuan, Z. Xie, J. Ma, W.J. Liu, D. Wang, W. Xu, E.C. Holmes, G.F. Gao, G. Wu, W. Chen, W. Shi, W. Tan, Genomic characterisation and epidemiology of 2019 novel coronavirus: implications for virus origins and receptor binding, Lancet 395 (2020) 565–574, https://doi.org/10.1016/S0140-6736(20)30251-8.
[39] M. Bouvet, C. Debarnot, I. Imbert, B. Selisko, E.J. Snijder, B. Canard, E. Decroly, In vitro reconstitution of SARS-coronavirus mRNA cap methylation, PLoS Pathog. 6 (2010), https://doi.org/10.1371/journal.ppat.1000863 e1000863-e1000863.
[40] G.C. Paesen, A. Collet, C. Sallamand, F. Debart, J.-J. Vasseur, B. Canard, E. Decroly, J.M. Grimes, X-ray structure and activities of an essential mononegavirales L-protein domain, Nature comm 6 (2015) 8749–8758, https://doi.org/10.1038/ncomms9749.